

Symmetric Positive Semi-definite Riemannian Geometry with Application to Domain Adaptation*

Or Yair[†], Almog Lahav[†], and Ronen Talmon[†]

Abstract. In this paper, we present new results on the Riemannian geometry of symmetric positive semi-definite (SPSD) matrices. First, based on an existing approximation of the geodesic path, we introduce approximations of the logarithmic and exponential maps. Second, we present a closed-form expression for Parallel Transport (PT). Third, we derive a canonical representation for a set of PSD matrices. Based on these results, we propose an algorithm for Domain Adaptation (DA) and demonstrate its performance in two applications: fusion of hyper-spectral images and motion identification.

Key words. Symmetric Positive Semi-definite, Parallel Transport, Domain Adaptation

AMS subject classifications. 62-07, 57M50, 53C22, 53C20, 53C21, 68T99.

1. Introduction. Recent technological advances give rise to the collection and storage of massive complex datasets. These datasets are often high dimensional and multimodal, calling for the development of informative representations. Since such complex data typically do not live in a Euclidean space, standard linear analysis techniques applied directly to the data are inappropriate. Consequently, analysis techniques based on Riemannian geometry have attracted significant research attention. While the basic mathematical operations used for data analysis, e.g., addition, subtraction, and comparison, are straight-forward in the Euclidean space, they are often non-trivial or intractable in particular Riemannian spaces.

A considerable amount of literature has been published on the Riemannian geometry of Symmetric Positive Definite (SPD) matrices, where it was shown to be useful for various applications, e.g., in computer vision, medical data analysis, and machine learning [26, 3, 18, 16, 2, 27, 28, 4]. For example, in [26], Pennec et al. introduced the use of the affine-invariant metric, facilitating closed-form expressions of the exponential and logarithmic maps, in medical imaging. In [3], Barachant et al. proposed an algorithm based on the Riemannian distance and the estimation of the Riemannian mean [23] of SPD matrices for brain computer interface (BCI). The PT on the SPD manifold, which has a closed-form expression, was used in [32] for DA. Similar geometric operations in other Riemannian spaces have been developed as well, e.g., on the Grassmann manifold [1] and on the Stiefel manifold [12], and were shown to be beneficial for a wide variety of data analysis tasks, e.g. [29].

In this paper, we consider the Riemannian geometry of symmetric positive semi-definite (SPSD) matrices. Formally, let $\mathcal{S}_{d,r}^+$ denote the set of $d \times d$ PSD matrices with a fixed rank $r < d$. Based on the eigenvalue decomposition, it can be shown that any PSD matrix

*Submitted to the editors DATE.

Funding: This work was funded by the European Unions Horizon 2020 research grant agreement 802735.

[†]Viterbi Faculty of Electrical Engineering, Technion, Israel Institute of Technology (oryair@campus.technion.ac.il), (ronen@ef.technion.ac.il.) O. Yair is supported by the Adams Fellowship Program of the Israel Academy of Sciences and Humanities

$\mathbf{C} \in \mathcal{S}_{d,r}^+$ can be represented by:

$$\mathbf{C} = \mathbf{G}\mathbf{P}\mathbf{G}^T$$

where $\mathbf{G} \in \mathbb{R}^{d \times r}$ has orthonormal columns representing a point on the Grassmann manifold and $\mathbf{P} \in \mathbb{R}^{r \times r}$ is an SPD matrix. This geometry extends the Riemannian geometry of SPD matrices. In addition, it facilitates the analysis of a larger pool of data features. For example, the SPD geometry supports the analysis of only full-rank covariance matrices. However, it is well known that in many real-world problems, this is not the case. Often, high-dimensional data such as gene expression data [20] and hyper-spectral imaging data [15, 25] have an intrinsic low-rank structure, and therefore, the associated covariance matrices are not full-rank. In addition to supporting low-rank covariance matrices, in contrast to the SPD geometry, the SPSD geometry applies to a wide variety of kernels, graph Laplacians, and similarity matrices, which are common data features in contemporary data analysis.

Despite the high relevance to many data analysis techniques, the usage of the Riemannian geometry of SPSD matrices has thus far been limited, since it lacks several pivotal components. First, there is no available explicit expression for the geodesic path in $\mathcal{S}_{d,r}^+$ connecting two SPSD matrices. As a consequence, there is no definitive expression for the Riemannian distance between two SPSD matrices, which is typically defined as the arc length of the geodesic path. In addition, basic operations such as the logarithmic and the exponential maps, which are derived from the geodesic path, are undefined. Second, the representation of $\mathbf{C} \in \mathcal{S}_{d,r}^+$ by a pair (\mathbf{G}, \mathbf{P}) is not unique, posing challenges when jointly analyzing multiple SPSD matrices. These missing components led to an avenue of research, where full-rank structure is imposed by adding a scalar matrix to each of the given low-rank matrices [30, 13]. Essentially, this approach “artificially” transforms the SPSD geometry into the SPD geometry by introducing a component that does not stem from the data.

Instead, here we propose to extend the Riemannian geometry of SPSD matrices head-on. Our developments largely rely on the work of Bonnabel and Sepulchre [7], where an approximation of the geodesic path on the SPSD manifold was presented, giving rise to a meaningful measure of proximity between two SPSD matrices, and on the work of Bonnabel et al. [6], where a rank-preserving mean of a set of fixed-rank SPSD matrices was defined. First, based on the approximation of the geodesic path in $\mathcal{S}_{d,r}^+$ [7], we introduce an approximation of the logarithmic and exponential maps. Second, we present a closed-form expression for the PT on $\mathcal{S}_{d,r}^+$. Finally, using the mean of SPSD matrices proposed in [6], we derive a canonical representation for a set of SPSD matrices.

Based on the developed mathematical infrastructure for the analysis of SPSD matrices with a fixed rank, we address the problem of DA. Often, due to the inherent heterogeneity of many types of datasets, useful representations usually cannot be achieved simply by considering the union of multiple datasets. We present an algorithm for DA, which is based on the PT on $\mathcal{S}_{d,r}^+$ and facilitates an informative representation of multiple heterogeneous datasets. We showcase the performance of our algorithm in two applications. First, we demonstrate fusion of hyper-spectral images collected by airborne sensors, which allows high-quality categorization of land-covers in one image by training a classifier on another image. Second, we show accurate motion identification based on recordings of motions, which is actor-independent, i.e., independent of the actor executing these motions.

The remainder of the paper is organized as follows. In [section 2](#) we present preliminaries on the Riemannian manifolds which are relevant to our work: the manifold of SPD matrices \mathcal{P}_d , the Grassman manifold $\mathcal{G}_{d,r}$ and the manifold of SPSP matrices with a fixed rank $\mathcal{S}_{d,r}^+$. In [section 3](#), we describe a particular transportation map on \mathcal{P}_d and $\mathcal{G}_{d,r}$ that is derived from PT. [Section 4](#) presents our approximations for the logarithmic and exponential maps on $\mathcal{S}_{d,r}^+$, the PT-driven transportation map on $\mathcal{S}_{d,r}^+$, and a canonical representation for a set of SPSP matrices. Next, we propose a new DA algorithm in [section 5](#). [Section 6](#) consists of two applications of the proposed DA algorithm to real data. Finally, [section 7](#) concludes the paper.

2. Preliminaries. In this section, we briefly describe several known properties of the manifold of SPD matrices \mathcal{P}_d , the Grassman manifold $\mathcal{G}_{d,r}$, and the manifold of SPSP matrices $\mathcal{S}_{d,r}^+$, which will be extensively used throughout the paper. First, we formally denote the following sets:

- \mathcal{P}_d – The set of $d \times d$ SPD matrices.
- $\mathcal{S}_{d,r}^+$ – The set of $d \times d$ SPSP matrices with rank $r \leq d$.
- $\mathcal{G}_{d,r}$ – The set of r -dimensional subspaces of \mathbb{R}^d .
- $\mathcal{V}_{d,r}$ – The set of $d \times r$ matrices with orthonormal columns: $\mathbf{U}^T \mathbf{U} = \mathbf{I}_r$ for $\mathbf{U} \in \mathcal{V}_{d,r}$.
- \mathcal{O}_d – The set of $d \times d$ orthogonal matrices $\mathcal{O}_d \cong \mathcal{V}_{d,d}$.

In addition, given a manifold \mathcal{M} with its Riemannian geodesic distance d_R , we denote the Fréchet (Karcher) mean \bar{x} of the set $\{x_i \in \mathcal{M}\}_i$ by:

$$\bar{x} = M(\{x_i\}) := \arg \min_{x \in \mathcal{M}} \sum_i d_R^2(x, x_i)$$

2.1. The manifold of SPD matrices \mathcal{P}_d . The matrix $\mathbf{P} \in \mathbb{R}^{d \times d}$ is an SPD matrix if it is symmetric and all of its eigenvalues are strictly positive. Denote the set of all $d \times d$ SPD matrices by:

$$\mathcal{P}_d = \left\{ \mathbf{P} \in \mathbb{R}^{d \times d} : \mathbf{P} = \mathbf{P}^T, \mathbf{P} \succ 0 \right\}$$

The set \mathcal{P}_d can be embedded in a $\frac{1}{2}d(d+1)$ dimensional space, that is:

$$\dim(\mathcal{P}_d) = \frac{1}{2}d(d+1)$$

The tangent space $\mathcal{T}_{\mathbf{P}}\mathcal{P}_d$ at any point $\mathbf{P} \in \mathcal{P}_d$ is the set of all symmetric matrices:

$$\mathcal{T}_{\mathbf{P}}\mathcal{P}_d = \left\{ \mathbf{S} \in \mathbb{R}^{d \times d} : \mathbf{S} = \mathbf{S}^T \right\}$$

The affine invariant metric (inner product) in the tangent space $\mathcal{T}_{\mathbf{P}}\mathcal{P}_d$ is given by:

$$(2.1) \quad \langle \mathbf{S}_1, \mathbf{S}_2 \rangle_{\mathbf{P}} = \left\langle \mathbf{P}^{-\frac{1}{2}} \mathbf{S}_1 \mathbf{P}^{-\frac{1}{2}}, \mathbf{P}^{-\frac{1}{2}} \mathbf{S}_2 \mathbf{P}^{-\frac{1}{2}} \right\rangle$$

for any $\mathbf{S}_1, \mathbf{S}_2 \in \mathcal{T}_{\mathbf{P}}\mathcal{P}_d$, where $\langle \cdot, \cdot \rangle$ is the standard Euclidean inner product given by $\langle \mathbf{A}, \mathbf{B} \rangle = \text{Tr} \{ \mathbf{A}^T \mathbf{B} \}$.

The set \mathcal{P}_d equipped with the affine invariant metric (2.1) gives rise to a Riemannian manifold. Below, we outline the main properties of this manifold. For more details, we refer the readers to [5].

- The geodesic path from $\mathbf{P}_1 \in \mathcal{P}_d$ to $\mathbf{P}_2 \in \mathcal{P}_d$ can be parametrized by:

$$(2.2) \quad \gamma_{\mathbf{P}_1 \rightarrow \mathbf{P}_2}^{\mathcal{P}}(t) = \mathbf{P}_1^{\frac{1}{2}} \left(\mathbf{P}_1^{-\frac{1}{2}} \mathbf{P}_2 \mathbf{P}_1^{-\frac{1}{2}} \right)^t \mathbf{P}_1^{\frac{1}{2}}, \quad t \in [0, 1]$$

- The arc length of the geodesic path defines an affine invariant distance and is explicitly given by:

$$d_{\mathcal{P}}^2(\mathbf{P}_1, \mathbf{P}_2) = \left\| \log \left(\mathbf{P}_1^{-\frac{1}{2}} \mathbf{P}_2 \mathbf{P}_1^{-\frac{1}{2}} \right) \right\|_F^2 = \sum_{i=1}^d \log^2(\lambda_i(\mathbf{P}_1^{-1} \mathbf{P}_2))$$

where $\lambda_i(\mathbf{A})$ is the i th eigenvalue of the matrix \mathbf{A} , and $\|\cdot\|_F$ is the Frobenius norm.

- The exponential map from the point $\mathbf{P} \in \mathcal{P}_d$ at the direction $\mathbf{S} \in \mathcal{T}_{\mathbf{P}}\mathcal{P}_d$ is given by:

$$(2.3) \quad \mathcal{P}_d \ni \text{Exp}_{\mathbf{P}}(\mathbf{S}) = \mathbf{P}^{\frac{1}{2}} \exp \left(\mathbf{P}^{-\frac{1}{2}} \mathbf{S} \mathbf{P}^{-\frac{1}{2}} \right) \mathbf{P}^{\frac{1}{2}}$$

- The logarithmic map, which is the inverse of the exponential map, is given by:

$$(2.4) \quad \mathcal{T}_{\mathbf{P}}\mathcal{P}_d \ni \text{Log}_{\mathbf{P}}(\mathbf{P}_0) = \mathbf{P}^{\frac{1}{2}} \log \left(\mathbf{P}^{-\frac{1}{2}} \mathbf{P}_0 \mathbf{P}^{-\frac{1}{2}} \right) \mathbf{P}^{\frac{1}{2}}$$

for any $\mathbf{P}, \mathbf{P}_0 \in \mathcal{P}_d$.

- The PT $\Gamma_{\mathbf{P}_1 \rightarrow \mathbf{P}_2} : \mathcal{T}_{\mathbf{P}_1}\mathcal{P}_d \rightarrow \mathcal{T}_{\mathbf{P}_2}\mathcal{P}_d$ of the tangent vector $\mathbf{S} \in \mathcal{T}_{\mathbf{P}_1}\mathcal{P}_d$ to $\mathcal{T}_{\mathbf{P}_2}\mathcal{P}_d$, is given by:

$$\Gamma_{\mathbf{P}_1 \rightarrow \mathbf{P}_2}(\mathbf{S}) = \mathbf{E} \mathbf{S} \mathbf{E}^T, \quad \mathbf{E} = (\mathbf{P}_2 \mathbf{P}_1^{-1})^{\frac{1}{2}}$$

- Given a set of SPD matrices $\{\mathbf{P}_i \in \mathcal{P}_d\}_i$, a useful Euclidean vector approximation in the tangent space $\mathcal{T}_{\bar{\mathbf{P}}}\mathcal{P}$, where $\bar{\mathbf{P}} = M(\{\mathbf{P}_i\})$, is given by:

$$d_{\mathcal{P}}(\mathbf{P}_i, \mathbf{P}_j) \underset{\geq}{\approx} \left\| \hat{\mathbf{S}}_i - \hat{\mathbf{S}}_j \right\|_F$$

$$\text{where } \hat{\mathbf{S}}_i = \bar{\mathbf{P}}^{-\frac{1}{2}} \text{Log}_{\bar{\mathbf{P}}}(\mathbf{P}_i) \bar{\mathbf{P}}^{-\frac{1}{2}} = \log \left(\bar{\mathbf{P}}^{-\frac{1}{2}} \mathbf{P}_i \bar{\mathbf{P}}^{-\frac{1}{2}} \right)$$

Given a set of SPD matrices $\{\mathbf{P}_i \in \mathcal{P}_d\}_i$, [Algorithm 2.1](#) can be used to obtain the Riemannian SPD mean $\bar{\mathbf{P}} = M(\{\mathbf{P}_i\})$.

Algorithm 2.1 SPD Mean

Input: A set of SPD matrices $\{\mathbf{P}_i \in \mathcal{P}_d\}_{i=1}^N$

Output: The Riemannian mean $\bar{\mathbf{P}} = M(\{\mathbf{P}_i\})$

1. **set** $\bar{\mathbf{P}} \leftarrow \frac{1}{N} \sum_{i=1}^N \mathbf{P}_i$
 2. **do**
 - (a) $\bar{\mathbf{S}} \leftarrow \frac{1}{N} \sum_{i=1}^N \text{Log}_{\bar{\mathbf{P}}}(\mathbf{P}_i)$ ▷ using (2.4)
 - (b) $\bar{\mathbf{P}} \leftarrow \text{Exp}_{\bar{\mathbf{P}}}(\bar{\mathbf{S}})$ ▷ using (2.3)
 - while** $\|\bar{\mathbf{S}}\|_F > \epsilon$
-

2.2. The Grassman manifold $\mathcal{G}_{d,r}$. Let

$$(2.5) \quad [Q] := \left\{ Q \begin{bmatrix} Q_r & \mathbf{0} \\ \mathbf{0} & Q_{d-r} \end{bmatrix} \mid Q \in \mathcal{O}_d, Q_r \in \mathcal{O}_r, Q_{d-r} \in \mathcal{O}_{d-r} \right\}$$

be the equivalence class of all orthogonal matrices such that their r leftmost columns span the same subspace. If $Q_1, Q_2 \in [Q]$, that is, the r leftmost columns have the same span, we denote the equivalence relation by:

$$(2.6) \quad Q_1, Q_2 \in [Q] \iff Q_1 \sim Q_2.$$

For convenience, when considering only the r leftmost columns of $Q \in \mathcal{O}_d$ we sometimes use $G \in \mathcal{V}_{d,r}$ (and similarly $[G]$) instead of Q (and $[Q]$), and we will state the dimensions explicitly when necessary. This “thin representation”, using G instead of Q , gives rise to economic implementations of most of the operations detailed below.

Let $\mathcal{G}_{d,r} = \{[Q]\}$ be the set of all r -dimensional subspaces of \mathbb{R}^d , where $[Q]$ represents any unique r -dimensional span as in (2.5). It can also be viewed as the quotient space

$$\mathcal{G}_{d,r} = \mathcal{O}_d / (\mathcal{O}_r \times \mathcal{O}_{d-r})$$

Following [12], for computational purposes, we usually consider a single matrix, either $G \in \mathcal{V}_{d,r}$ or $Q \in \mathcal{O}_d$, to represent the entire equivalence class $[Q]$. Throughout the paper, when considering multiple points (subspaces) on the Grassman manifold, we assume that the principal angles between those subspaces are strictly smaller than $\frac{\pi}{2}$.

The set $\mathcal{G}_{d,r}$ can be embedded in a $r(d-r)$ dimensional space, that is:

$$\dim(\mathcal{G}_{d,r}) = r(d-r)$$

The tangent space $\mathcal{T}_Q \mathcal{G}_{d,r}$ at $[Q] \in \mathcal{G}_{d,r}$, represented by the orthogonal matrix $Q \in \mathcal{O}_d$, is given by:

$$\mathcal{T}_Q \mathcal{G}_{d,r} = \left\{ \Delta \in \mathbb{R}^{d \times d} \mid \Delta = QB^{\text{skew}} \right\}$$

where $B^{\text{skew}} = \begin{bmatrix} \mathbf{0} & -B^T \\ B & \mathbf{0} \end{bmatrix}$ for any $B \in \mathbb{R}^{(d-r) \times r}$. For simplicity, the tangent space $\mathcal{T}_Q \mathcal{G}_{d,r}$ can be equivalently written as

$$\mathcal{T}_G \mathcal{G}_{d,r} = \left\{ G_\perp B \in \mathbb{R}^{d \times r} \mid B \in \mathbb{R}^{(d-r) \times r} \right\}$$

where $Q = \begin{bmatrix} G & G_\perp \end{bmatrix}$, $G \in \mathcal{V}_{d,r}$, and $G_\perp \in \mathcal{V}_{d,d-r}$ is the orthogonal complement of G . The inner product in $\mathcal{T}_Q \mathcal{G}_{d,r}$ is given by:

$$(2.7) \quad \langle \Delta_1, \Delta_2 \rangle_Q = \frac{1}{2} \langle \Delta_1, \Delta_2 \rangle = \langle B_1, B_2 \rangle$$

where $\Delta_i = QB_i^{\text{skew}} \in \mathcal{T}_Q \mathcal{G}_{d,r}$.

The set $\mathcal{G}_{d,r}$ and the inner product (2.7) form the Grassman manifold. Below, we outline its main properties. For more details, we refer the readers to [12].

- The exponential map from the point $\mathbf{Q} \in \mathcal{O}_d$, which represents the point $[\mathbf{Q}] \in \mathcal{G}_{d,r}$, at the direction $\mathbf{\Delta} = \mathbf{Q}\mathbf{B}^{\text{skew}} \in \mathcal{T}_{\mathbf{Q}}\mathcal{G}_{d,r}$ is given by:

$$(2.8) \quad \text{Exp}_{\mathbf{Q}}(\mathbf{\Delta}) = \mathbf{Q} \exp(\mathbf{B}^{\text{skew}})$$

where $[\text{Exp}_{\mathbf{Q}}(\mathbf{\Delta})] \in \mathcal{G}_{d,r}$. For small values of t , the curve $[\text{Exp}_{\mathbf{Q}}(t\mathbf{\Delta})]$ is a geodesic. Similarly, the exponential map from the point $\mathbf{G} \in \mathcal{V}_{d,r}$, which represents the point $[\mathbf{G}] \in \mathcal{G}_{d,r}$, at the direction $\mathbf{G}_{\perp}\mathbf{B} \in \mathcal{T}_{\mathbf{G}}\mathcal{G}_{d,r}$ is given by:

$$(2.9) \quad \text{Exp}_{\mathbf{G}}(\mathbf{G}_{\perp}\mathbf{B}) = (\mathbf{G}\mathbf{V} \cos(\mathbf{\Sigma}) + \mathbf{U} \sin(\mathbf{\Sigma})) \mathbf{V}^T$$

where $\mathbf{G}_{\perp}\mathbf{B} = \mathbf{U}\mathbf{\Sigma}\mathbf{V}$ is a compact SVD.

- Given two points $\mathbf{G}, \mathbf{G}_0 \in \mathcal{V}_{d,r}$, representing the two points $[\mathbf{G}], [\mathbf{G}_0] \in \mathcal{G}_{d,r}$, the logarithmic map, which is the inverse of the exponential map, is given by:

$$(2.10) \quad \mathcal{T}_{\mathbf{G}}\mathcal{G}_{d,r} \ni \text{Log}_{\mathbf{G}}(\mathbf{G}_0) = \mathbf{U} \arctan(\mathbf{\Sigma}) \mathbf{V}^T$$

where

$$(\mathbf{I} - \mathbf{G}\mathbf{G}^T) \mathbf{G}_0 (\mathbf{G}^T \mathbf{G}_0)^{-1} = \mathbf{U}\mathbf{\Sigma}\mathbf{V}^T$$

is a compact SVD decomposition. Let $\mathbf{Q} = [\mathbf{G} \ \mathbf{G}_{\perp}]$ and $\mathbf{Q}_0 = [\mathbf{G}_0, \mathbf{G}_{0,\perp}]$. The tangent vector in (2.10) can be recast as

$$(2.11) \quad \mathcal{T}_{\mathbf{Q}}\mathcal{G}_{d,r} \ni \text{Log}_{\mathbf{Q}}(\mathbf{Q}_0) = \mathbf{\Delta} = \mathbf{Q}\mathbf{B}_0^{\text{skew}}$$

where $\mathbf{B}_0^{\text{skew}} = \begin{bmatrix} \mathbf{0} & -\mathbf{B}_0^T \\ \mathbf{B}_0 & \mathbf{0} \end{bmatrix}$ and $\text{Log}_{\mathbf{G}}(\mathbf{G}_0) = \mathbf{G}_{\perp}\mathbf{B}_0$.

- Given $\mathbf{G}_1, \mathbf{G}_2 \in \mathcal{V}_{d,r}$, the geodesic between the two points can be computed by:

$$(2.12) \quad \gamma_{\mathbf{G}_1 \rightarrow \mathbf{G}_2}^{\mathcal{G}}(t) = \text{Exp}_{\mathbf{G}_1}(t \text{Log}_{\mathbf{G}_1}(\mathbf{G}_2)), \quad t \in [0, 1]$$

Note that in general $\gamma_{\mathbf{G}_1 \rightarrow \mathbf{G}_2}^{\mathcal{G}}(1) \sim \mathbf{G}_2$ but not necessarily $\gamma_{\mathbf{G}_1 \rightarrow \mathbf{G}_2}^{\mathcal{G}}(1) = \mathbf{G}_2$. We note that the expression in (2.12) is well defined if all the principal angles between the two subspaces $[\mathbf{G}_1]$ and $[\mathbf{G}_2]$ are strictly smaller than $\frac{\pi}{2}$.

- The arc length of the geodesic path between the points $[\mathbf{G}_1] \in \mathcal{G}_{d,r}$ and $[\mathbf{G}_2] \in \mathcal{G}_{d,r}$ is given by:

$$d_{\mathcal{G}}(\mathbf{G}_1, \mathbf{G}_2) = \|\mathbf{\Theta}\|_F$$

where $\mathbf{G}_1^T \mathbf{G}_2 = \mathbf{O}_1 (\cos \mathbf{\Theta}) \mathbf{O}_2^T$ is an SVD decomposition, $\mathbf{O}_1, \mathbf{O}_2 \in \mathcal{O}_r$, $\mathbf{\Theta} = \text{diag}([\theta_1, \theta_2, \dots, \theta_r])$, and $\{\theta_i\}$ are known as the principal angles between the two subspaces $[\mathbf{G}_1]$ and $[\mathbf{G}_2]$.

- The PT of the tangent vector $\mathbf{\Delta} = \mathbf{Q}\mathbf{B}^{\text{skew}} \in \mathcal{T}_{\mathbf{Q}}\mathcal{G}_{d,r}$ along the geodesic $\text{Exp}_{\mathbf{Q}}(t\tilde{\mathbf{\Delta}})$

where $\tilde{\mathbf{\Delta}} = \mathbf{Q}\tilde{\mathbf{B}}^{\text{skew}} \in \mathcal{T}_{\mathbf{Q}}\mathcal{G}_{d,r}$ is given by:

$$(2.13) \quad \begin{aligned} \Gamma_{\mathbf{Q} \rightarrow \text{Exp}_{\mathbf{Q}}(t\mathbf{\Delta})}(\mathbf{\Delta}) &= \text{Exp}_{\mathbf{Q}}(t\tilde{\mathbf{\Delta}}) \mathbf{Q}^T \mathbf{\Delta} \\ &= \mathbf{Q} \exp(t\tilde{\mathbf{B}}^{\text{skew}}) \mathbf{B}^{\text{skew}} \in \mathcal{T}_{\text{Exp}_{\mathbf{Q}}(t\mathbf{\Delta})}\mathcal{G}_{d,r} \end{aligned}$$

Specifically, if $\tilde{\mathbf{Q}} = \text{Exp}_{\mathbf{Q}}(\tilde{\mathbf{\Delta}}) = \mathbf{Q} \exp(\tilde{\mathbf{B}}^{\text{skew}})$ we have:

$$\Gamma_{\mathbf{Q} \rightarrow \tilde{\mathbf{Q}}}(\mathbf{\Delta}) = \tilde{\mathbf{Q}}\mathbf{B}^{\text{skew}}$$

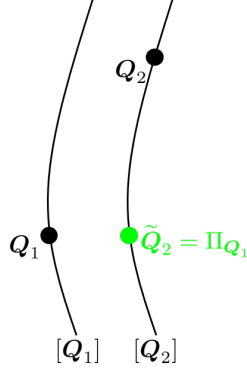


Figure 1: Illustration of the computation of the closest point in $[Q_2]$ to Q_1 in (2.14).

Given a set of matrices $\{Q_i \in \mathcal{O}_d\}_i$, where each represents a point $[Q_i] \in \mathcal{G}_{d,r}$, [Algorithm 2.2](#) can be used to obtain the Riemannian mean on the Grassman manifold $\overline{Q} = M(\{Q_i\})$.

Let $Q_1 \in \mathcal{O}_d$ and $Q_2 \in \mathcal{O}_d$ represent two points on $\mathcal{G}_{d,r}$, and let $G_1 \in \mathcal{V}_{d,r}$ and $G_2 \in \mathcal{V}_{d,r}$ be their r leftmost columns, respectively. When considering the Stiefel manifold $\mathcal{V}_{d,r} = \mathcal{O}_d / \mathcal{O}_{d-r}$, the closest point \tilde{Q}_2 in $[Q_2]$ to Q_1 is given by:

$$(2.14) \quad \tilde{Q}_2 = \Pi_{Q_1}(Q_2) := \text{Exp}_{Q_1}(\text{Log}_{Q_1}(Q_2)) = \text{Exp}_{Q_1}(Q_1 B_2^{\text{skew}}) = Q_1 \exp(B_2^{\text{skew}})$$

where the logarithmic map is computed using (2.10) and (2.11), and the exponential map is computed using (2.8). See [Figure 1](#) for illustration. Using the compact representations G_1 and G_2 , (2.14) can be simply recast as

$$(2.15) \quad \tilde{G}_2 = \Pi_{G_1}(G_2) := \text{Exp}_{G_1}(\text{Log}_{G_1}(G_2)) = G_2 O_2 O_1^T$$

where $G_1^T G_2 = O_1 \Sigma O_2^T$ is an SVD decomposition. This result will be heavily used in remainder of the paper.

Algorithm 2.2 Grassman Mean

Input: A set of matrices $\{G_i \in \mathcal{V}_{d,r}\}_i$, each represents a point $[G_i] \in \mathcal{G}_{d,r}$

Output: The Grassman mean $\overline{G} = M(\{G_i\})$

1. **set** $\overline{G} \leftarrow G_1$

2. **do**

(a) $\overline{\Delta} \leftarrow \frac{1}{N} \sum_{i=1}^N \text{Log}_{\overline{G}}(Q_i)$

▷ using (2.10)

(b) $\overline{G} \leftarrow \text{Exp}_{\overline{G}}(\overline{\Delta})$

▷ using (2.9)

while $\|\overline{\Delta}\|_F > \epsilon$

2.3. The manifold of SPSP $\mathcal{S}_{d,r}^+$. The set of all $d \times d$ SPSP matrices with a fixed rank $r < d$ is given by

$$\mathcal{S}_{d,r}^+ = \left\{ C \in \mathbb{R}^{d \times d} : C = C^T, C \succeq 0, \text{rank}(C) = r \right\}$$

Since any $\mathbf{C} \in \mathcal{S}_{d,r}^+$ can be represented by:

$$\mathbf{C} = \mathbf{G}\mathbf{P}\mathbf{G}^T$$

where $\mathbf{G} \in \mathcal{V}_{d,r}$ and $\mathbf{P} \in \mathcal{P}_r$, Bonnabel and Sepulchre [7] proposed the following structure space representation

$$\mathbf{C} \cong (\mathbf{G}, \mathbf{P})$$

We note that this representation is not unique since

$$\mathbf{C} = \mathbf{G}\mathbf{P}\mathbf{G}^T = (\mathbf{G}\mathbf{O}) (\mathbf{O}^T \mathbf{P} \mathbf{O}) (\mathbf{G}\mathbf{O})^T$$

and therefore

$$\mathbf{C} \cong (\mathbf{G}\mathbf{O}, \mathbf{O}^T \mathbf{P} \mathbf{O})$$

for any $\mathbf{O} \in \mathcal{O}_r$. In other words, the set $\mathcal{S}_{d,r}^+$ can be written as the quotient manifold

$$\mathcal{S}_{d,r}^+ \cong (\mathcal{V}_{d,r} \times \mathcal{P}_r) / \mathcal{O}_r$$

Using the structure space, the set $\mathcal{S}_{d,r}^+$ can be embedded in $rd - \frac{1}{2}r(r-1)$ dimensional space, that is:

$$\dim(\mathcal{S}_{d,r}^+) = rd - \frac{1}{2}r(r-1)$$

The tangent space $\mathcal{T}_{(\mathbf{G}, \mathbf{P})}\mathcal{S}_{d,r}^+$ in the structure space is given by:

$$\mathcal{T}_{(\mathbf{G}, \mathbf{P})}\mathcal{S}_{d,r}^+ = \{(\mathbf{\Delta}, \mathbf{S}) : \mathbf{\Delta} \in \mathcal{T}_{\mathbf{G}}\mathcal{G}_{d,r}, \mathbf{S} \in \mathcal{T}_{\mathbf{P}}\mathcal{P}_r\}$$

The inner product in the tangent space $\mathcal{T}_{(\mathbf{G}, \mathbf{P})}\mathcal{S}_{d,r}^+$ is given by:

$$(2.16) \quad \langle (\mathbf{\Delta}_1, \mathbf{S}_1), (\mathbf{\Delta}_2, \mathbf{S}_2) \rangle_{(\mathbf{G}, \mathbf{P})} = \langle \mathbf{\Delta}_1, \mathbf{\Delta}_2 \rangle_{\mathbf{G}} + k \langle \mathbf{S}_1, \mathbf{S}_2 \rangle_{\mathbf{P}}, \quad k > 0$$

where $(\mathbf{\Delta}_i, \mathbf{S}_i) \in \mathcal{T}_{(\mathbf{G}, \mathbf{P})}\mathcal{S}_{d,r}^+$.

There is no definitive expression for the geodesic path between two points on the manifold. Bonnabel and Sepulchre [7] proposed the following approximation in the structure space. Let $\mathbf{C}_1 \cong (\mathbf{G}_1, \mathbf{P}_1)$ and $\mathbf{C}_2 \cong (\mathbf{G}_2, \mathbf{P}_2)$ be two points on $\mathcal{S}_{d,r}^+$ such that $\mathbf{G}_2 := \Pi_{\mathbf{G}_1}(\mathbf{G}_2)$. Then, the approximate geodesic path between \mathbf{C}_1 and \mathbf{C}_2 is given by:

$$(2.17) \quad \tilde{\gamma}_{\mathbf{C}_1 \rightarrow \mathbf{C}_2}(t) = \mathbf{G}(t) \mathbf{P}(t) \mathbf{G}^T(t), \quad t \in [0, 1]$$

where $\mathbf{G}(t) = \gamma_{\mathbf{G}_1 \rightarrow \mathbf{G}_2}^{\mathcal{G}}(t)$ and $\mathbf{P}(t) = \gamma_{\mathbf{P}_1 \rightarrow \mathbf{P}_2}^{\mathcal{P}}(t)$ as in (2.2) and (2.12). In addition, the length of the curve $\tilde{\gamma}_{\mathbf{C}_1 \rightarrow \mathbf{C}_2}$ is given by:

$$(2.18) \quad l^2(\tilde{\gamma}_{\mathbf{C}_1 \rightarrow \mathbf{C}_2}) = d_{\mathcal{G}}^2(\mathbf{G}_1, \mathbf{G}_2) + k d_{\mathcal{P}}^2(\mathbf{P}_1, \mathbf{P}_2), \quad k > 0$$

We note that this is not a distance on $\mathcal{S}_{d,r}^+$, since it does not satisfy the triangle inequality. For more details on the SPSP manifold, we refer the readers to [7].

Given a set of SPSP matrices $\{\mathbf{C}_i \in \mathcal{S}_{d,r}^+\}_i$, an algorithm to compute a point which admits the desirable property of the geometric mean was proposed in [6]. The algorithm is summarized in Algorithm 2.3.

We remark that the lack of definitive expression for the geodesic path entails that there is also no definitive expression for the logarithmic and exponential maps.

Algorithm 2.3 Riemannian Mean of SPSPD matrices as proposed in [6]

Input: A set of SPSPD matrices $\{C_i \in \mathcal{S}_{d,r}^+\}_{i=1}^N$

Output: The proposed mean $\bar{C} = \overline{GPG}^T$

1. Obtain the Grassman mean \bar{G} :
 - (a) Obtain $G_i \in \mathcal{V}_{d,r}$, the range of C_i (e.g., by using SVD)
 - (b) Compute $\bar{G} \in \mathcal{V}_{d,r}$, the Grassman mean of $\{G_i\}_{i=1}^N$ \triangleright using Algorithm 2.2
2. Obtain the SPD mean \bar{P} :
 - (a) Compute O_i and \bar{O}_i using SVD:

$$G_i^T \bar{G} = O_i \Sigma_i \bar{O}_i$$

- (b) Set $P_i = \bar{O}_i O_i^T G_i^T C_i G_i O_i \bar{O}_i^T \in \mathcal{P}_r$
 - (c) Compute $\bar{P} = M(\{P_i\})$, the SPD mean of $\{P_i\}_{i=1}^N$ \triangleright using Algorithm 2.1
 3. Set $\bar{C} = \bar{G} \bar{P} \bar{G}^T$
-

3. Transportation on a Riemannian manifold. In this section, we study a transport map of a set of points with respect to two reference points on a Riemannian manifold. This transportation gives the foundation to the proposed DA, as we will show in the sequel. We begin with a general definition.

Definition 3.1. Consider a set of points $\mathcal{X} = \{x_i \in \mathcal{M}\}_{i=1}^{N_x}$ on a Riemannian manifold \mathcal{M} . Let $\bar{x} = M(\mathcal{X})$ be the Riemannian mean of the set, and let $\bar{y} \in \mathcal{M}$ be a target mean.

We call a transport map $\varphi_{\bar{x} \rightarrow \bar{y}} : \mathcal{M} \rightarrow \mathcal{M}$ an isometric transport of \mathcal{X} from \bar{x} to \bar{y} , if it satisfies the following two properties.

1. $\varphi_{\bar{x} \rightarrow \bar{y}}$ preserves pairwise distances: $d(x_i, x_j) = d(\varphi_{\bar{x} \rightarrow \bar{y}}(x_i), \varphi_{\bar{x} \rightarrow \bar{y}}(x_j))$.
2. The mean of the transported set is \bar{y} , that is $M(\{\varphi_{\bar{x} \rightarrow \bar{y}}(x_i)\}) = \bar{y}$.

By the above definition, given such a transport map $\varphi_{\bar{x} \rightarrow \bar{y}}$, any composition of “rotation” about \bar{y} (in the Riemannian sense) applied to $\varphi_{\bar{x} \rightarrow \bar{y}}(\mathcal{X})$ also satisfied Definition 3.1.

In order to resolve this degree of freedom, we focus on transport maps defined as follows. Let $\Gamma_{\bar{x} \rightarrow \bar{y}} : \mathcal{T}_{\bar{x}}\mathcal{M} \rightarrow \mathcal{T}_{\bar{y}}\mathcal{M}$ be the PT from $\mathcal{T}_{\bar{x}}\mathcal{M}$ to $\mathcal{T}_{\bar{y}}\mathcal{M}$ on the manifold \mathcal{M} . Based on $\Gamma_{\bar{x} \rightarrow \bar{y}}$, we define the transport map $\Gamma_{\bar{x} \rightarrow \bar{y}}^+ : \mathcal{M} \rightarrow \mathcal{M}$ as follows

$$\tilde{x}_i = \Gamma_{\bar{x} \rightarrow \bar{y}}^+(x_i) := \text{Exp}_{\bar{y}}(\Gamma_{\bar{x} \rightarrow \bar{y}}(\text{Log}_{\bar{x}}(x_i))),$$

for any $x_i \in \mathcal{X}$. Namely, the map $\Gamma_{\bar{x} \rightarrow \bar{y}}^+$ is a composition of three steps:

1. Applying the logarithmic map to x_i and obtaining the corresponding vector $\xi_i \in \mathcal{T}_{\bar{x}}\mathcal{M}$:

$$\xi_i = \text{Log}_{\bar{x}}(x_i).$$

2. Applying PT to ξ_i from $\mathcal{T}_{\bar{x}}\mathcal{M}$ to $\mathcal{T}_{\bar{y}}\mathcal{M}$:

$$\tilde{\xi}_i = \Gamma_{\bar{x} \rightarrow \bar{y}}(\xi_i).$$

3. Applying the exponential map to $\tilde{\xi}_i$ and obtaining the point $\tilde{x}_i \in \mathcal{M}$:

$$\tilde{x}_i = \text{Exp}_{\bar{y}}(\tilde{\xi}_i).$$

This transport is derived from PT with one important distinction: while PT maps points from tangent space to tangent space, this transport maps points from the manifold to the manifold.

The extra degree of freedom associated with [Definition 3.1](#) is resolved by considering the map $\Gamma_{\bar{x} \rightarrow \bar{y}}^+$, because the parallel transports $\Gamma_{\bar{x} \rightarrow \bar{y}}$ we consider on the specific manifolds of interest are with respect to the Levi-Civita connection. The Levi-Civita connection is the unique torsion-free metric connection. As a result, such parallel transports along a curve are torsion-free, i.e., they preserve the inner products on the various tangent spaces, circumventing the “screw around the curve”.

In the following, we will show that the specifications of $\Gamma_{\bar{x} \rightarrow \bar{y}}^+$ to the manifolds \mathcal{P}_d and $\mathcal{G}_{d,r}$ satisfy [Definition 3.1](#). In addition, we will provide compact and closed-form expressions for these transports.

3.1. Γ^+ on \mathcal{P}_d . Let $\mathcal{X} = \{\mathbf{P}_i \in \mathcal{P}_d\}_{i=1}^{N_x}$ be a set of points on \mathcal{P}_d with mean $M(\mathcal{X}) = \bar{\mathbf{P}} \in \mathcal{P}_d$, and let $\bar{\mathbf{R}} \in \mathcal{P}_d$ be a target mean. In [\[32\]](#), it was shown that $\Gamma_{\bar{\mathbf{P}} \rightarrow \bar{\mathbf{R}}}^+ : \mathcal{P}_d \rightarrow \mathcal{P}_d$ can be written in a compact (linear) form:

$$(3.1) \quad \Gamma_{\bar{\mathbf{P}} \rightarrow \bar{\mathbf{R}}}^+(\mathbf{P}_i) = \mathbf{E} \mathbf{P}_i \mathbf{E}^T,$$

where

$$(3.2) \quad \mathbf{E} = \left(\overline{\mathbf{R} \mathbf{P}}^{-1} \right)^{\frac{1}{2}} = \bar{\mathbf{P}}^{\frac{1}{2}} \left(\bar{\mathbf{P}}^{-\frac{1}{2}} \overline{\mathbf{R} \mathbf{P}}^{-\frac{1}{2}} \right)^{\frac{1}{2}} \bar{\mathbf{P}}^{-\frac{1}{2}}.$$

Direct computation yields that $\Gamma_{\bar{\mathbf{P}} \rightarrow \bar{\mathbf{R}}}^+$ admits the properties of [Definition 3.1](#). First, $\Gamma_{\bar{\mathbf{P}} \rightarrow \bar{\mathbf{R}}}^+$ is isometric, i.e., it preserves the pairwise distances; for any $\mathbf{P}_1, \mathbf{P}_2 \in \mathcal{P}_d$

$$d_{\mathcal{P}_d} \left(\Gamma_{\bar{\mathbf{P}} \rightarrow \bar{\mathbf{R}}}^+(\mathbf{P}_1), \Gamma_{\bar{\mathbf{P}} \rightarrow \bar{\mathbf{R}}}^+(\mathbf{P}_2) \right) = d_{\mathcal{P}_d} (\mathbf{E} \mathbf{P}_1 \mathbf{E}^T, \mathbf{E} \mathbf{P}_2 \mathbf{E}^T) = d_{\mathcal{P}_d} (\mathbf{P}_1, \mathbf{P}_2),$$

where the latter transition is because $d_{\mathcal{P}_d}$ is affine invariant. Second, the mean of the transported set coincides with the target mean, that is

$$(3.3) \quad \begin{aligned} M \left(\Gamma_{\bar{\mathbf{P}} \rightarrow \bar{\mathbf{R}}}^+(\mathcal{X}) \right) &= M (\mathbf{E} \mathcal{X} \mathbf{E}^T) \stackrel{(*)}{=} \mathbf{E} M(\mathcal{X}) \mathbf{E}^T \\ &= \mathbf{E} \bar{\mathbf{P}} \mathbf{E}^T \stackrel{(**)}{=} \bar{\mathbf{P}}^{\frac{1}{2}} \left(\bar{\mathbf{P}}^{-\frac{1}{2}} \overline{\mathbf{R} \mathbf{P}}^{-\frac{1}{2}} \right) \bar{\mathbf{P}}^{\frac{1}{2}} = \bar{\mathbf{R}} \end{aligned}$$

where in $(*)$ we use the congruence invariance property of geometric mean (see [\[5\]](#)), and in $(**)$ we plug [\(3.2\)](#).

Suppose that $\bar{\mathbf{R}}$ is the Riemannian mean of another set $\mathcal{Y} = \{\mathbf{R}_i \in \mathcal{P}_d\}_{i=1}^{N_x}$. In addition to satisfying [Definition 3.1](#), the transported set $\{\Gamma_{\bar{\mathbf{P}} \rightarrow \bar{\mathbf{R}}}^+(\mathbf{P}_i) \mid \mathbf{P}_i \in \mathcal{X}\}_{i=1}^{N_x}$ coincides with \mathcal{Y} under the conditions specified in the following statement.

Proposition 3.2. *Let $\{\mathbf{P}_i\}_i$ be a set of points on \mathcal{P}_d with the Riemannian mean $\bar{\mathbf{P}}$. Consider the map $t : \mathcal{P}_d \rightarrow \mathcal{P}_d$ defined by*

$$\mathbf{R}_i = t(\mathbf{P}_i) = \mathbf{T} \mathbf{P}_i \mathbf{T}^T$$

where $\mathbf{T} \in \text{GL}_d$. Let $\bar{\mathbf{R}}$ be the Riemannian mean of the resulting set $\{\mathbf{R}_i\}_i$. The following holds

$$\Gamma_{\bar{\mathbf{P}} \rightarrow \bar{\mathbf{R}}}^+(\mathbf{P}_i) = \mathbf{R}_i, \quad \forall i$$

if and only if \mathbf{T} is of the form $\mathbf{T} = \bar{\mathbf{P}}^{\frac{1}{2}} \mathbf{B} \bar{\mathbf{P}}^{-\frac{1}{2}}$ where either $\mathbf{B} \succ 0$ or $\mathbf{B} \prec 0$.

See the proof in the Supplementary Material (SM).

Note that on \mathcal{P}_d , one can overload the PT operator $\Gamma_{\bar{\mathbf{P}} \rightarrow \bar{\mathbf{R}}}$ with the manifold transportation $\Gamma_{\bar{\mathbf{P}} \rightarrow \bar{\mathbf{R}}}^+$, that is

$$(3.4) \quad \Gamma_{\bar{\mathbf{P}} \rightarrow \bar{\mathbf{R}}}^+(\mathbf{P}_i) = \Gamma_{\bar{\mathbf{P}} \rightarrow \bar{\mathbf{R}}}(\mathbf{P}_i) = \mathbf{E} \mathbf{P}_i \mathbf{E}^T.$$

3.2. Γ^+ on $\mathcal{G}_{d,r}$. Let $\mathcal{X} = \{[\mathbf{Q}]_i \in \mathcal{G}_{d,r}\}_{i=1}^{N_x}$ be a set of points on $\mathcal{G}_{d,r}$ with mean $M(\mathcal{X}) = [\bar{\mathbf{Q}}]$, and let $[\bar{\mathbf{V}}] \in \mathcal{G}_{d,r}$ be a target mean. On the Grassman manifold, we have an equivalent result to (3.4), giving rise to a closed-form expression of $\Gamma_{\bar{\mathbf{Q}} \rightarrow \bar{\mathbf{V}}}^+$.

Proposition 3.3. Let $\bar{\mathbf{Q}} \in [\bar{\mathbf{Q}}]$ and $\bar{\mathbf{V}} \in [\bar{\mathbf{V}}]$ be two points in \mathcal{O}_d , such that $\bar{\mathbf{V}} = \Pi_{\bar{\mathbf{Q}}}(\bar{\mathbf{V}})$. Define $\Gamma_{\bar{\mathbf{Q}} \rightarrow \bar{\mathbf{V}}}^+ : \mathcal{G}_{d,r} \rightarrow \mathcal{G}_{d,r}$ by

$$(3.5) \quad \Gamma_{\bar{\mathbf{Q}} \rightarrow \bar{\mathbf{V}}}^+(\mathbf{Q}_i) = \text{Exp}_{\bar{\mathbf{V}}} \left(\Gamma_{\bar{\mathbf{Q}} \rightarrow \bar{\mathbf{V}}}(\text{Log}_{\bar{\mathbf{Q}}}(\mathbf{Q}_i)) \right)$$

Then

$$(3.6) \quad \Gamma_{\bar{\mathbf{Q}} \rightarrow \bar{\mathbf{V}}}^+(\mathbf{Q}_i) \sim \Gamma_{\bar{\mathbf{Q}} \rightarrow \bar{\mathbf{V}}}(\mathbf{Q}_i) = \bar{\mathbf{V}} \bar{\mathbf{Q}}^T \mathbf{Q}_i$$

where \sim is the equivalent class as in (2.6), and if \mathbf{Q}_i is chosen such that $\mathbf{Q}_i = \Pi_{\bar{\mathbf{Q}}}(\mathbf{Q}_i)$, then the equivalence becomes equality:

$$(3.7) \quad \Gamma_{\bar{\mathbf{Q}} \rightarrow \bar{\mathbf{V}}}^+(\mathbf{Q}_i) = \Gamma_{\bar{\mathbf{Q}} \rightarrow \bar{\mathbf{V}}}(\mathbf{Q}_i) = \bar{\mathbf{V}} \bar{\mathbf{Q}}^T \mathbf{Q}_i$$

See the proof in the SM. We remark that in (3.5), we apply the map $\Gamma_{\bar{\mathbf{Q}} \rightarrow \bar{\mathbf{V}}}^+$ to a matrix $\mathbf{Q}_i \in \mathcal{O}_d$ in $[\mathbf{Q}_i]$, rather than to $[\mathbf{Q}_i]$. Similarly, the range of the map is also written as if it is in \mathcal{O}_d rather than in $\mathcal{G}_{d,r}$. For simplicity, we continue with this slight abuse of notation throughout the paper.

Using Proposition 3.3, we show that $\Gamma_{\bar{\mathbf{Q}} \rightarrow \bar{\mathbf{V}}}^+$ satisfies the properties of Definition 3.1. First, from (3.6), since $\bar{\mathbf{Q}}, \bar{\mathbf{V}} \in \mathcal{O}_d$, $\Gamma_{\bar{\mathbf{Q}} \rightarrow \bar{\mathbf{V}}}^+$ is a unitary transformation, and therefore it preserves the pairwise distances. That is

$$d_{\mathcal{G}} \left(\Gamma_{\bar{\mathbf{Q}} \rightarrow \bar{\mathbf{V}}}^+(\mathbf{Q}_1), \Gamma_{\bar{\mathbf{Q}} \rightarrow \bar{\mathbf{V}}}^+(\mathbf{Q}_2) \right) = d_{\mathcal{G}}(\mathbf{Q}_1, \mathbf{Q}_2).$$

Second, the mean of the transported set coincides with the target mean. Namely

$$(3.8) \quad M \left(\Gamma_{\bar{\mathbf{Q}} \rightarrow \bar{\mathbf{V}}}^+(\mathcal{X}) \right) = M \left(\bar{\mathbf{V}} \bar{\mathbf{Q}}^T \mathcal{X} \right) \underset{(*)}{=} \bar{\mathbf{V}} \bar{\mathbf{Q}}^T M(\mathcal{X}) = \bar{\mathbf{V}} \bar{\mathbf{Q}}^T \bar{\mathbf{Q}} = \bar{\mathbf{V}}$$

where $(*)$ is due to the fact that the mean of a rotated set is the rotated mean (see [6]).

In the spirit of the three steps comprising Γ^+ , the maps $\Gamma_{\overline{\mathbf{P}} \rightarrow \overline{\mathbf{R}}}^+$ on the \mathcal{P}_d and $\Gamma_{\overline{\mathbf{Q}} \rightarrow \overline{\mathbf{V}}}^+$ on $\mathcal{G}_{d,r}$ can be recast as three steps defined on the respective manifolds rather than via the tangent planes. On \mathcal{P} , using (3.1) and (3.2) we can write

$$(3.9) \quad \Gamma_{\overline{\mathbf{P}} \rightarrow \overline{\mathbf{R}}}^+ = f_{\mathcal{P}}^{-1} \circ g_{\mathcal{P}} \circ f_{\mathcal{P}}$$

where

$$f_{\mathcal{P}}(\mathbf{P}_i) = \overline{\mathbf{P}}^{-\frac{1}{2}} \mathbf{P}_i \overline{\mathbf{P}}^{-\frac{1}{2}}$$

and

$$g_{\mathcal{P}}(\mathbf{P}_i) = \left(\overline{\mathbf{P}}^{-\frac{1}{2}} \overline{\mathbf{R}} \overline{\mathbf{P}}^{-\frac{1}{2}} \right)^{\frac{1}{2}} \mathbf{P}_i \left(\overline{\mathbf{P}}^{-\frac{1}{2}} \overline{\mathbf{R}} \overline{\mathbf{P}}^{-\frac{1}{2}} \right)^{\frac{1}{2}}$$

Similarly on \mathcal{G} , using (2.13) we can write

$$(3.10) \quad \Gamma_{\overline{\mathbf{Q}} \rightarrow \overline{\mathbf{V}}}^+ = f_{\mathcal{G}}^{-1} \circ g_{\mathcal{G}} \circ f_{\mathcal{G}}$$

where

$$f_{\mathcal{G}}(\mathbf{Q}_i) = \overline{\mathbf{Q}}^T \mathbf{Q}_i$$

and

$$g_{\mathcal{G}}(\mathbf{Q}_i) = \overline{\mathbf{Q}}^T \overline{\mathbf{V}} \mathbf{Q}_i$$

On both manifolds, the map f transports the cloud of points to the identity (so the new mean is \mathbf{I}), and the map g transports the cloud from the identity to “ $\overline{\mathbf{R}}$ over $\overline{\mathbf{P}}$ ”, namely $\left(\overline{\mathbf{P}}^{-\frac{1}{2}} \overline{\mathbf{R}} \overline{\mathbf{P}}^{-\frac{1}{2}} \right)^{\frac{1}{2}}$, on \mathcal{P}_d , and to “ $\overline{\mathbf{V}}$ over $\overline{\mathbf{Q}}$ ”, namely $\overline{\mathbf{Q}}^{-1} \overline{\mathbf{V}} = \overline{\mathbf{Q}}^T \overline{\mathbf{V}}$ (since $\overline{\mathbf{Q}} \in \mathcal{O}_d$), on $\mathcal{G}_{d,r}$. Finally, f^{-1} maps the cloud to $\overline{\mathbf{R}}$ (on \mathcal{P}_d) and $\overline{\mathbf{V}}$ (on $\mathcal{G}_{d,r}$).

4. Transportation on $\mathcal{S}_{d,r}^+$. In this section we derive a transportation $\tilde{\Gamma}^+ : \mathcal{S}_{d,r}^+ \rightarrow \mathcal{S}_{d,r}^+$ in a similar manner to Γ^+ on \mathcal{P}_d and $\mathcal{G}_{d,r}$, which are presented in subsection 3.1 and subsection 3.2, respectively. Given two points $\overline{\mathbf{C}}, \overline{\mathbf{Y}} \in \mathcal{S}_{d,r}^+$, let $\tilde{\Gamma}^+ : \mathcal{S}_{d,r}^+ \rightarrow \mathcal{S}_{d,r}^+$ be a composition of three steps: (i) projection to the tangent space $\mathcal{T}_{\overline{\mathbf{C}}} \mathcal{S}_{d,r}^+$, (ii) transportation between the two tangent spaces $\mathcal{T}_{\overline{\mathbf{C}}} \mathcal{S}_{d,r}^+ \rightarrow \mathcal{T}_{\overline{\mathbf{Y}}} \mathcal{S}_{d,r}^+$, and (iii) projection back from $\mathcal{T}_{\overline{\mathbf{Y}}} \mathcal{S}_{d,r}^+$ to the manifold $\mathcal{S}_{d,r}^+$. The implementation used in subsection 3.1 and subsection 3.2 comprises the logarithmic map, PT and the exponential map. However, the logarithmic and the exponential maps in $\mathcal{S}_{d,r}^+$ have no explicit expressions, and there are no existing numerical methods to compute these operators. Therefore, here we propose approximations of these operators, which in turn facilitate the construction of a transportation $\tilde{\Gamma}^+ : \mathcal{S}_{d,r}^+ \rightarrow \mathcal{S}_{d,r}^+$, which could be viewed as the counterpart of Γ^+ from section 3 on $\mathcal{S}_{d,r}^+$. However, in contrast to Γ^+ , since there is no known method to compute the geodesic distance on $\mathcal{S}_{d,r}^+$, $\tilde{\Gamma}^+$ is not guaranteed to admit the isometry property in Definition 3.1. Nevertheless, we will show that $\tilde{\Gamma}^+$ is useful for DA, similarly to Γ^+ on \mathcal{P}_d [32].

4.1. Operations on $\mathcal{S}_{d,r}^+$. The maps Γ^+ on \mathcal{P}_d and $\mathcal{G}_{d,r}$ require the exponential and the logarithmic maps as well as PT, which are derived from the geodesics. Here, we present approximations to the logarithmic map and to the exponential map on $\mathcal{S}_{d,r}^+$ based on the approximation of the geodesic given in (2.17). The presented approximations make use of the structure space representation introduced in subsection 2.3, that is, any SPSP matrix $\mathbf{C}_i \in \mathcal{S}_{d,r}^+$ can be represented as $\mathbf{C}_i \cong (\mathbf{G}_i, \mathbf{P}_i)$ where $\mathbf{G}_i \in \mathcal{V}_{d,r}$ and $\mathbf{P}_i \in \mathcal{P}_r$.

Formally, given the curve $\tilde{\gamma}_{(\mathbf{G}_1, \mathbf{P}_1) \rightarrow (\mathbf{G}_2, \mathbf{P}_2)}(t)$ between the two points $(\mathbf{G}_1, \mathbf{P}_1)$ and $(\mathbf{G}_2, \mathbf{P}_2)$ such that $\mathbf{G}_2 = \Pi_{\mathbf{G}_1}(\mathbf{G}_2)$ as in (2.17), we define an approximate of the logarithmic map $\tilde{\mathbf{L}}_{(\mathbf{G}_1, \mathbf{P}_1)} : \mathcal{S}_{d,r}^+ \rightarrow \mathcal{T}_{(\mathbf{G}_1, \mathbf{P}_1)}\mathcal{S}_{d,r}^+$ using the derivative of $\tilde{\gamma}$ (rather than the geodesic):

$$\begin{aligned} \tilde{\mathbf{L}}_{(\mathbf{G}_1, \mathbf{P}_1)}(\mathbf{G}_2, \mathbf{P}_2) &= \dot{\tilde{\gamma}}_{(\mathbf{G}_1, \mathbf{P}_1) \rightarrow (\mathbf{G}_2, \mathbf{P}_2)}(0) \\ (4.1) \quad &= \left(\dot{\gamma}_{\mathbf{G}_1 \rightarrow \mathbf{G}_2}^{\mathcal{G}}(0), \dot{\gamma}_{\mathbf{P}_1 \rightarrow \mathbf{P}_2}^{\mathcal{P}}(0) \right) \\ &= (\text{Log}_{\mathbf{G}_1}(\mathbf{G}_2), \text{Log}_{\mathbf{P}_1}(\mathbf{P}_2)) \end{aligned}$$

Accordingly, an approximate of the exponential map $\tilde{\mathbf{E}}_{(\mathbf{G}_1, \mathbf{P}_1)} : \mathcal{T}_{(\mathbf{G}_1, \mathbf{P}_1)}\mathcal{S}_{d,r}^+ \rightarrow \mathcal{S}_{d,r}^+$, which is the inverse map of the approximate logarithmic map, is given by:

$$(4.2) \quad \tilde{\mathbf{E}}_{(\mathbf{G}_1, \mathbf{P}_1)}(\Delta, \mathbf{S}) = \tilde{\mathbf{L}}^{-1}(\Delta, \mathbf{S}) = (\text{Exp}_{\mathbf{G}_1}(\Delta), \text{Exp}_{\mathbf{P}_1}(\mathbf{S}))$$

where $(\Delta, \mathbf{S}) \in \mathcal{T}_{(\mathbf{G}_1, \mathbf{P}_1)}\mathcal{S}_{d,r}^+$.

Lastly, the PT, denoted by $\Gamma_{(\mathbf{G}_1, \mathbf{P}_1) \rightarrow (\mathbf{G}_2, \mathbf{P}_2)} : \mathcal{T}_{(\mathbf{G}_1, \mathbf{P}_1)}\mathcal{S}_{d,r}^+ \rightarrow \mathcal{T}_{(\mathbf{G}_2, \mathbf{P}_2)}\mathcal{S}_{d,r}^+$, can be expressed explicitly without any approximation:

$$(4.3) \quad \Gamma_{(\mathbf{G}_1, \mathbf{P}_1) \rightarrow (\mathbf{G}_2, \mathbf{P}_2)}(\Delta, \mathbf{S}) = (\Gamma_{\mathbf{G}_1 \rightarrow \mathbf{G}_2}(\Delta), \Gamma_{\mathbf{P}_1 \rightarrow \mathbf{P}_2}(\mathbf{S}))$$

for any $(\Delta, \mathbf{S}) \in \mathcal{T}_{(\mathbf{G}_1, \mathbf{P}_1)}\mathcal{S}_{d,r}^+$.

Seemingly, equipped with the three operations defined above, we are ready for the construction of the transportation $\tilde{\Gamma}^+$ on $\mathcal{S}_{d,r}^+$. However, the expression in (4.1) is true only when $\mathbf{G}_2 = \Pi_{\mathbf{G}_1}(\mathbf{G}_2)$. Therefore, in subsection 4.2 we verify that this condition is met, and in subsection 4.3 we present the construction of $\tilde{\Gamma}^+$.

4.2. Canonical representation. Let $\mathcal{C} = \left\{ \mathbf{C}_i \in \mathcal{S}_{d,r}^+ \mid \mathbf{C}_i \cong (\mathbf{U}_i, \mathbf{T}_i) \right\}_{i=1}^N$ be a set of SPSP matrices with some arbitrary structure space representation $\mathbf{C}_i \cong (\mathbf{U}_i, \mathbf{T}_i)$. Recall that the structure space representation is not unique, that is $\mathbf{C}_i \cong (\mathbf{U}_i, \mathbf{T}_i) \cong (\mathbf{U}_i \mathbf{O}_i^T, \mathbf{O}_i \mathbf{T}_i \mathbf{O}_i^T)$ for any $\mathbf{O}_i \in \mathcal{O}_r$. Let $[\mathbf{G}] = M(\{[\mathbf{U}_i]\})$ be the Grassman mean of the ranges of the SPSP matrices $\{\mathbf{C}_i\}$. In this subsection, we reduce the number of degrees of freedom stemming from the possible arbitrary choice of $\{\mathbf{O}_i\}_{i=1}^N$ by fixing a representative matrix $\overline{\mathbf{G}} \in [\mathbf{G}]$ (any representative will do) and deriving a structure space representation $\mathbf{C}_i \cong (\mathbf{G}_i, \mathbf{P}_i)$ such that $\mathbf{G}_i = \Pi_{\overline{\mathbf{G}}}(\mathbf{G}_i)$. This particular structure space representation allows us to apply (4.1) to the set \mathcal{C} .

Formally, let $\overline{\mathbf{C}} \in \mathcal{S}_{d,r}^+$ be the Riemannian mean of \mathcal{C} on $\mathcal{S}_{d,r}^+$, and let $\overline{\mathbf{G}} \in [\mathbf{G}]$ where both means can be obtained by Algorithm 2.3. Set $\overline{\mathbf{P}} = \overline{\mathbf{G}}^T \overline{\mathbf{C}} \overline{\mathbf{G}} \in \mathcal{P}_r$ such that $\overline{\mathbf{C}} \cong (\overline{\mathbf{G}}, \overline{\mathbf{P}})$, and consider the following canonical representation

$$(4.4) \quad \mathbf{C}_i \cong (\mathbf{G}_i, \mathbf{P}_i)$$

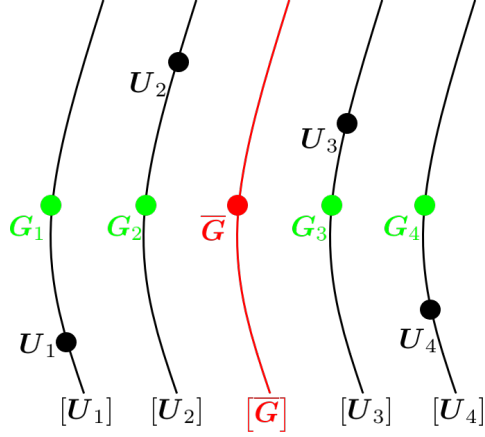


Figure 2: Illustration of the canonical representation. $[\bar{\mathbf{G}}]$ is the mean of the set $\{[\mathbf{U}_i]\}$. We peak a representative $\bar{\mathbf{G}}$ (red point) and rotate each \mathbf{U}_i to \mathbf{G}_i (green points) such that $\mathbf{G}_i = \Pi_{\bar{\mathbf{G}}}(\mathbf{G}_i) = \Pi_{\bar{\mathbf{G}}}(\mathbf{U}_i)$.

where $\mathbf{G}_i = \Pi_{\bar{\mathbf{G}}}(\mathbf{U}_i)$, and $\mathbf{P}_i = \mathbf{G}_i^T \mathbf{C}_i \mathbf{G}_i$. This ‘alignment’ procedure is illustrated in Figure 2.

The proposed canonical representation (4.4) admits the following properties. First, since $\mathbf{G}_i \sim \mathbf{U}_i$ for all i , the mean $\bar{\mathbf{G}}$ of $\{\mathbf{U}_i\}_i$ coincides with the mean of $\{\mathbf{G}_i\}_i$, namely, $[\bar{\mathbf{G}}] = M(\{[\mathbf{U}_i]\}) = M(\{[\mathbf{G}_i]\})$. Second, as shown in [6], it follows from Algorithm 2.3 that the mean of $\{\mathbf{P}_i\}$ is indeed $\bar{\mathbf{P}} = M(\{\mathbf{P}_i\}_i)$.

In addition, after applying the approximate logarithmic map $\tilde{\mathbf{L}}$ (4.1) to the set \mathcal{C} , the vectors in the tangent space $\mathcal{T}_{(\bar{\mathbf{G}}, \bar{\mathbf{P}})} \mathcal{S}_{d,r}^+$ are centered around the origin. This stems from the above two properties. Specifically, taking the arithmetic mean of vectors obtained by applying $\tilde{\mathbf{L}}$ to the canonical representations $\{(\mathbf{G}_i, \mathbf{P}_i)_i\}$ results in

$$(4.5) \quad \frac{1}{N} \sum_{i=1}^N \tilde{\mathbf{L}}_{(\bar{\mathbf{G}}, \bar{\mathbf{P}})}(\mathbf{G}_i, \mathbf{P}_i) = \frac{1}{N} \left(\sum_{i=1}^N \log_{\bar{\mathbf{G}}}(\mathbf{G}_i), \sum_{i=1}^N \log_{\bar{\mathbf{P}}}(\mathbf{P}_i) \right) = (\mathbf{0}, \mathbf{0})$$

since the arithmetic means of the vectors in $\mathcal{T}_{\bar{\mathbf{G}}} \mathcal{G}_{d,r}$ and $\mathcal{T}_{\bar{\mathbf{P}}} \mathcal{P}_r$, namely $\sum_{i=1}^N \log_{\bar{\mathbf{G}}}(\mathbf{G}_i)$ and $\sum_{i=1}^N \log_{\bar{\mathbf{P}}}(\mathbf{P}_i)$, lie at the origin, because $\bar{\mathbf{G}} = M(\{[\mathbf{G}_i]\})$ and $\bar{\mathbf{P}} = M(\{\mathbf{P}_i\})$, respectively. Importantly, since the obtained vectors are centered at the origin, they can provide an approximation of the points $(\mathbf{G}_i, \mathbf{P}_i)$ in a linear vector space.

4.3. $\tilde{\Gamma}^+$ on $\mathcal{S}_{d,r}^+$. Let $\tilde{\Gamma}_{\bar{\mathbf{C}} \rightarrow \bar{\mathbf{Y}}}^+(\mathbf{C}_i)$ denote a transport of the set \mathcal{C} from its mean $\bar{\mathbf{C}} \cong (\bar{\mathbf{G}}, \bar{\mathbf{P}})$ to a new center of mass $\bar{\mathbf{Y}} \cong (\bar{\mathbf{V}}, \bar{\mathbf{R}})$. Suppose $\bar{\mathbf{C}} \cong (\bar{\mathbf{G}}, \bar{\mathbf{P}})$ is the canonical representation and suppose that $\bar{\mathbf{V}} = \Pi_{\bar{\mathbf{G}}}(\bar{\mathbf{V}})$ and $\bar{\mathbf{R}} = \bar{\mathbf{V}}^T \bar{\mathbf{Y}} \bar{\mathbf{V}}$.

With the above preparation, define:

$$\begin{aligned}
 \tilde{\Gamma}_{\overline{C} \rightarrow \overline{Y}}^+ (C_i) &\cong \tilde{\Gamma}_{(\overline{G}, \overline{P}) \rightarrow (\overline{V}, \overline{R})}^+ (G_i, P_i) \\
 &:= \left(\Gamma_{\overline{G} \rightarrow \overline{V}}^+ (G_i), \Gamma_{\overline{P} \rightarrow \overline{R}}^+ (P_i) \right) \\
 &= \left(\overline{OQ}^T G_i, E P_i E^T \right) \\
 &\cong \overline{OQ}^T G_i E P_i E^T G_i^T Q O^T
 \end{aligned}
 \tag{4.6}$$

where $C_i \cong (G_i, P_i)$ is the canonical representation (see (4.4)), \overline{Q} is an orthogonal completion of \overline{G} , \overline{O} is an orthogonal completion of \overline{V} such that $\overline{O} = \Pi_{\overline{Q}}(\overline{O})$ (see (2.14)), and $E = \left(\overline{R} P^{-1} \right)^{\frac{1}{2}}$.

Since $M(\{O G_i\}_i) = \overline{V}$ and $M(\{E P_i E^T\}_i) = \overline{R}$ (see (3.3) and (3.8), respectively), the mean of the transported set $\tilde{\Gamma}^+(\mathcal{C})$ is indeed $M(\tilde{\Gamma}^+(\mathcal{C})) = \overline{Y} \cong (\overline{V}, \overline{R})$ satisfying property 2 in Definition 3.1.

5. Domain adaptation on $\mathcal{S}_{d,r}^+$. Consider two sets $\mathcal{X} = \{x_i \in \mathcal{M}\}_{i=1}^{N_x}$ and $\mathcal{Y} = \{y_j \in \mathcal{M}\}_{j=1}^{N_y}$, on a Riemannian manifold \mathcal{M} . Suppose the two sets are intrinsically homogeneous but concentrated on different parts of the manifold, and thus, the two sets can be viewed as if they live in different domains. To concur with the literature on DA, we will call \mathcal{X} the source domain and \mathcal{Y} the target domain. Multiple factors can contribute to this nuisance difference between the sets, such as different acquisition systems, sensing equipment, environments, and configurations, to name but a few. The goal of DA is to mitigate the difference between the two sets and to provide a new representation of their union, such that any subsequent processing and analysis applied to the union could be unaware of their original partition and could treat them as one homogeneous set.

For this purpose of DA, when the data lie on \mathcal{P}_d , it was shown that applying Γ^+ to one set, transporting the data from its Riemannian mean to the Riemannian mean of the other set, gives rise to the desired outcome [32]. Analogously, when the data lie on $\mathcal{G}_{d,r}$, one could apply Γ^+ on $\mathcal{G}_{d,r}$ in a similar manner, and arguably, could expect similar performance as Γ^+ on \mathcal{P}_d , since the two variants of Γ^+ satisfy the two properties of Definition 3.1, making them useful for DA. Namely, on \mathcal{P}_d and on $\mathcal{G}_{d,r}$, the transportation is “rigid”, that is, Γ^+ preserves pairwise distances and “matches” the means.

Here, we propose to utilize $\tilde{\Gamma}^+$ derived in subsection 4.3 for DA on $\mathcal{S}_{d,r}^+$. As discussed in section 4, there is no definitive way to compute the pairwise distances on $\mathcal{S}_{d,r}^+$, and therefore, $\tilde{\Gamma}^+$ is not guaranteed to admit property 1 of Definition 3.1. Nevertheless, it does satisfy property 2, and, as we show in section 6, it indeed facilitates a useful DA on the manifold of SPSP matrices.

Let \overline{X} and \overline{Y} be the Riemannian means of $\mathcal{X} = \{X_i \in \mathcal{S}_{d,r}^+\}_{i=1}^{N_x}$ and $\mathcal{Y} = \{Y_j \in \mathcal{S}_{d,r}^+\}_{j=1}^{N_y}$, respectively. Let $\overline{X} \cong (\overline{G}, \overline{P})$ and $X_i \cong (G_i, P_i)$ be the canonical representation of the mean and the SPSP matrices in \mathcal{X} in the structure space as in (4.4). In addition, let $\overline{V} \in \mathcal{V}_{d,r}$ be

the Grassman mean of the ranges of the SPSD matrices in \mathcal{Y} such that $\bar{\mathbf{V}} = \Pi_{\bar{\mathcal{G}}}(\bar{\mathbf{V}})$. Denote

$$\bar{\mathbf{R}} := \bar{\mathbf{V}}^T \bar{\mathbf{Y}} \bar{\mathbf{V}}$$

so that

$$\bar{\mathbf{Y}} \cong (\bar{\mathbf{V}}, \bar{\mathbf{R}})$$

These representations led in (4.6) to the following explicit form of $\tilde{\Gamma}_{\bar{\mathbf{X}} \rightarrow \bar{\mathbf{Y}}}^+$

$$\tilde{\Gamma}_{\bar{\mathbf{X}} \rightarrow \bar{\mathbf{Y}}}^+(\mathbf{X}_i) = \overline{\mathbf{OQ}}^T \mathbf{G}_i \mathbf{E} \mathbf{P}_i \mathbf{E}^T \mathbf{G}_i^T \overline{\mathbf{QO}}^T$$

With the above preparation, the proposed DA algorithm culminates in the application of $\tilde{\Gamma}_{\bar{\mathbf{X}} \rightarrow \bar{\mathbf{Y}}}^+$ to every SPSD matrix \mathbf{X}_i in \mathcal{X} , obtaining a new representation $\tilde{\mathbf{X}}_i$. The complete DA algorithm is given in Algorithm 5.1.

The proposed algorithm has several important features for DA. (i) The algorithm does not require many data points, because the computation of $\tilde{\Gamma}^+$ only depends on coarse estimates of the two means $\bar{\mathbf{X}} = M(\mathcal{X})$ and $\bar{\mathbf{Y}} = M(\mathcal{Y})$. (ii) Once $\tilde{\Gamma}^+$ is computed, it can be applied to new unseen data. Let \mathbf{X}^* be a new (unseen) point obtained from the source domain, then $\tilde{\mathbf{X}}^* = \tilde{\Gamma}_{\bar{\mathbf{X}} \rightarrow \bar{\mathbf{Y}}}^+(\mathbf{X}^*)$ is the corresponding out of sample extension. (iii) The extension of the algorithm to multiple data sets is straight-forward. When more than two sets are given, one set can be designated as a reference (target) set, and then, all the remaining (source) sets are transported (one-by-one) to that reference set. Recall that $\tilde{\Gamma}^+$ is completely unsupervised, namely, no labels are required. Hence, any set can be chosen as the reference set.

One shortcoming of the algorithm is that it makes use only of the first order statistics. Namely, if two source sets \mathcal{X}_1 and \mathcal{X}_2 have different high order statistics but share the same mean $\bar{\mathbf{X}}_1 = \bar{\mathbf{X}}_2$, the transportations $\tilde{\Gamma}_{\bar{\mathbf{X}}_1 \rightarrow \bar{\mathbf{Y}}}^+$ and $\tilde{\Gamma}_{\bar{\mathbf{X}}_2 \rightarrow \bar{\mathbf{Y}}}^+$ (to $\bar{\mathbf{Y}}$) are identical. For large data sets, where higher order statistics can be accurately estimated, we outline two possible modifications. First, based on [22], the proposed algorithm can be supplemented with a second moments alignment step. Specifically, recall that $\tilde{\Gamma}^+$ is a composition of three steps: (i) projection to the tangent space, (ii) application of PT, and (iii) projection back to the manifold. Let $\left\{ \left(\tilde{\Delta}_i, \tilde{\mathbf{S}}_i \right) \in \mathcal{T}_{(\bar{\mathbf{V}}, \bar{\mathbf{R}})} \mathcal{S}_{d,r}^+ \right\}_{i=1}^{N_x}$ be the tangent vectors obtained after step (ii). Instead of projecting back to the manifold at step (iii), we propose to project the target set \mathcal{Y} to $\mathcal{T}_{(\bar{\mathbf{V}}, \bar{\mathbf{R}})} \mathcal{S}_{d,r}^+$ as well. Now, the sets (the transported source set and the projected target set) are points in a vector space. This allow us to rotate the source set $\left\{ \left(\tilde{\Delta}_i, \tilde{\mathbf{S}}_i \right) \in \mathcal{T}_{(\bar{\mathbf{V}}, \bar{\mathbf{R}})} \mathcal{S}_{d,r}^+ \right\}_{i=1}^{N_x}$ such that its second moments are aligned with the second moments of the target set. In order to overcome the ambiguity in the orientation of the rotation, in [22], it was proposed to rotate each axis according to the smaller angle.

The second modification is based on [10] and [33], where DA is carried out by solving a regularized optimal transport problem [9]. There, the cost is based on the (squared) length of the curve $\tilde{\gamma}_{\mathbf{X}_i \rightarrow \mathbf{Y}_j}$, and the transportation is applied using a weighted mean. Since the length of the curve $\tilde{\gamma}$ is not a metric and the weighted mean on $\mathcal{S}_{d,r}^+$ needs to be developed, we postpone the development of this transportation to future work. We note that such a transformation does not aim to preserve pairwise distances, but rather, to align the respective distributions of the two sets \mathcal{X} and \mathcal{Y} .

Algorithm 5.1 DA on $\mathcal{S}_{d,r}^+$

Input: Two sets of SPSPD matrices $\mathcal{X} = \{\mathbf{X}_i \in \mathcal{S}_{d,r}^+\}_{i=1}^{N_x}$ and $\mathcal{Y} = \{\mathbf{Y}_i \in \mathcal{S}_{d,r}^+\}_{i=1}^{N_y}$.

Output: The set $\tilde{\mathcal{X}} = \{\tilde{\mathbf{X}}_i \in \mathcal{S}_{d,r}^+\}_{i=1}^{N_x}$ adapted to the domain of \mathcal{Y} .

1. Obtain the means of \mathcal{X} and \mathcal{Y} :
 - (a) Compute the SPSPD and Grassman means of \mathcal{X} and \mathcal{Y} \triangleright using [Algorithm 2.3](#)
 - i. $\bar{\mathbf{X}} \in \mathcal{S}_{d,r}^+$ and $\bar{\mathbf{G}} \in \mathcal{V}_{d,r}$ for \mathcal{X}
 - ii. $\bar{\mathbf{Y}} \in \mathcal{S}_{d,r}^+$ and $\bar{\mathbf{V}} \in \mathcal{V}_{d,r}$ for \mathcal{Y}
 - (b) Set $\bar{\mathbf{V}} \leftarrow \Pi_{\bar{\mathbf{G}}}(\bar{\mathbf{V}})$ \triangleright using [\(2.15\)](#)
 - (c) Set $\bar{\mathbf{P}} = \bar{\mathbf{G}}^T \bar{\mathbf{X}} \bar{\mathbf{G}}$ and $\bar{\mathbf{R}} = \bar{\mathbf{V}}^T \bar{\mathbf{Y}} \bar{\mathbf{V}}$
2. For $i = 1, 2, \dots, N_x$:
 - (a) Compute the canonical representation: $\mathbf{X}_i \cong (\mathbf{G}_i, \mathbf{P}_i)$ such that $\mathbf{G}_i = \Pi_{\bar{\mathbf{G}}}(\mathbf{G}_i)$ \triangleright see [\(4.4\)](#)
 - (b) Compute (\triangleright see [\(4.6\)](#)):

$$(\tilde{\mathbf{G}}_i, \tilde{\mathbf{P}}_i) = \tilde{\Gamma}_{(\bar{\mathbf{G}}, \bar{\mathbf{P}}) \rightarrow (\bar{\mathbf{V}}, \bar{\mathbf{R}})}^+ (\mathbf{G}_i, \mathbf{P}_i) = (\bar{\mathbf{O}} \bar{\mathbf{Q}}^T \mathbf{G}_i, \mathbf{E} \mathbf{P}_i \mathbf{E}^T)$$

where $\bar{\mathbf{Q}}$ is an orthogonal completion of $\bar{\mathbf{G}}$, $\bar{\mathbf{O}}$ is an orthogonal completion of $\bar{\mathbf{V}}$ such that $\bar{\mathbf{O}} = \Pi_{\bar{\mathbf{Q}}}(\bar{\mathbf{O}})$ (see [\(2.14\)](#)), and $\mathbf{E} = (\bar{\mathbf{R}} \bar{\mathbf{P}}^{-1})^{\frac{1}{2}}$.

(c) Set:

$$\tilde{\mathbf{X}}_i = \tilde{\mathbf{G}}_i \tilde{\mathbf{P}}_i \tilde{\mathbf{G}}_i^T$$

6. Experimental study.

6.1. Hyper-spectral imaging. To demonstrate our proposed algorithm for DA we apply it to a real hyper-spectral dataset. Hyper-Spectral Imaging (HSI) measures multiple spectral bands of the light reflected from a spatial area. Recent technological advances allow for the acquisition of hundreds of spectral bands which encode rich information on the captured scene. Therefore, a large and growing number of studies have addressed the challenge of analyzing and processing hyper-spectral images for various purposes, such as classification [\[11, 13, 14\]](#), change detection [\[31\]](#) and target detection [\[19\]](#).

A well known problem in analyzing two or more hyper-spectral images is the inherent diversity between different images. This diversity could be the result of differences in illumination, viewing angle, sensor configuration, and even the type of sensors. In order to analyze two different images, or to exploit the model learned from one image, say, $\mathbf{I}^{(1)}$, for analysis tasks in another image, say, $\mathbf{I}^{(2)}$, DA is required. We next explain how we apply our approach to this purpose.

Consider a hyper-spectral image organized in a 3D cube $\mathbf{I} \in \mathbb{R}^{n_x \times n_y \times n_b}$, which is also referred as the hyper-spectral cube, where n_x and n_y are the spatial dimensions and n_b is the number of spectral bands. Let $\mathbf{p}_i \in \mathbb{R}^{n_b}$, $i = 1, 2, \dots, n_x n_y$, be the i_{th} pixel of \mathbf{I} representing

a local spectral signature. Recently, it was shown in [13] that a good spatial-spectral feature of \mathbf{p}_i , which expresses the relations between the spectral bands, is the local covariance matrix $\mathbf{X}_i \in \mathbb{R}^{n_b \times n_b}$, given by:

$$(6.1) \quad \mathbf{X}_i = \frac{1}{|\mathcal{N}_i| - 1} \sum_{\mathbf{p}_j \in \mathcal{N}_i} (\mathbf{p}_j - \boldsymbol{\mu}_i) (\mathbf{p}_j - \boldsymbol{\mu}_i)^T$$

where \mathcal{N}_i are the J nearest neighbors of \mathbf{p}_i from all the pixels in a patch of size $W \times W$ centered at \mathbf{p}_i , and $\boldsymbol{\mu}_i = \frac{1}{|\mathcal{N}_i|} \sum_{\mathbf{p}_j \in \mathcal{N}_i} \mathbf{p}_j$. The nearest neighbors are chosen with respect to the angular (cosine) similarity:

$$\theta_{ij} = \arccos \left(\frac{\mathbf{p}_i^T \mathbf{p}_j}{\|\mathbf{p}_i\|_2 \|\mathbf{p}_j\|_2} \right)$$

A common assumption in HSI is that the spectral signature \mathbf{p}_i is a linear combination of a small number $r < n_b$ of spectral profiles [34, 17]. According to this assumption, \mathbf{X}_i is an SPSD matrix with rank r . Therefore, we can use our approach to adapt two (or more) hyper-spectral images $\mathbf{I}^{(1)} \in \mathbb{R}^{n_x^{(1)} \times n_y^{(1)} \times n_b}$ and $\mathbf{I}^{(2)} \in \mathbb{R}^{n_x^{(2)} \times n_y^{(2)} \times n_b}$ as follows: (i) Compute the local covariance matrices $\mathcal{X}^{(1)} = \{\mathbf{X}_i^{(1)} \in \mathcal{S}_{n_b, r}^+ \}_{i=1}^{n_x^{(1)} n_y^{(1)}}$, of pixels from $\mathbf{I}^{(1)}$ and the local covariance matrices $\mathcal{X}^{(2)} = \{\mathbf{X}_i^{(2)} \in \mathcal{S}_{n_b, r}^+ \}_{i=1}^{n_x^{(2)} n_y^{(2)}}$, of pixels from $\mathbf{I}^{(2)}$. (ii) Transport $\mathcal{X}^{(1)}$ to the domain of $\mathcal{X}^{(2)}$ by applying Algorithm 5.1 (giving rise to $\tilde{\mathcal{X}}^{(1)}$).

We apply our method for the purpose of adapting hyper-spectral images of the same scene but with different time of acquisition, taken from the Greeding dataset [14]. After removing rows and columns with non-valid pixels, the dimensions of the images are $n_x = 626$, $n_y = 591$ and $n_b = 127$. Figure 3 shows an RGB representation (3 channels) of two images from the Greeding dataset: **Greeding_Village1_refl**, denoted by $\mathbf{I}^{(1)}$, and **Greeding_Village3_refl**, denoted by $\mathbf{I}^{(2)}$. It can be visually observed that at least the illumination in these two images is different.

For the local covariance computation in (6.1), we use the same parameters as in [13]: patch size $W = 25$, number of neighbor pixels $J = 220$, and we set the rank to be $r = 40$ because empirically it attains good performance. A similar rank was reported in [13]. To reduce the computational load of Algorithm 5.1, we use subsets of 500 matrices $\mathcal{X}_s^{(1)} \subset \mathcal{X}^{(1)}$ and $\mathcal{X}_s^{(2)} \subset \mathcal{X}^{(2)}$ chosen randomly for the mean computation in step 1(a), instead of the entire sets.

In order to use a feasible amount of memory, after applying Algorithm 5.1 we represent each SPSD matrix only by its 40 principal components computed as follows: (i) compute the logarithmic map approximation in (4.1) for each $\mathbf{X} \in \mathcal{X}^{(1)} \cup \mathcal{X}^{(2)}$, (ii) compute the 40 principal directions of $\mathcal{X}_s^{(1)} \cup \mathcal{X}_s^{(2)}$ in the tangent space, and (iii) project each vector in the tangent space on the obtained principal directions.

The obtained DA is evaluated by using 6 land-cover labels from the Greeding dataset: dark roof, red roof, concrete, soil, grass and tree. We denote the set of local covariance matrices in $\mathbf{I}^{(1)}$ after applying Algorithm 5.1 by $\tilde{\mathcal{X}}^{(1)}$. Figure 4(a) and Figure 4(b) show the two principal components (PC) of 400 matrices from $\mathcal{X}^{(1)} \cup \mathcal{X}^{(2)}$ and $\tilde{\mathcal{X}}^{(1)} \cup \mathcal{X}^{(2)}$ respectively, where points



Figure 3: RGB representation (3 channels) of the two hyperspectral images $\mathbf{I}^{(1)}$ and $\mathbf{I}^{(2)}$, from the Greiding dataset [14].

are colored according to the land-cover labels. As can be seen in Figure 4(a), points from $\mathcal{X}^{(1)}$, marked by circles, and points from $\mathcal{X}^{(2)}$, marked by asterisks, with the same label (color) reside in different regions. Conversely, in Figure 4(b), after applying Algorithm 5.1, we observe that points both from $\tilde{\mathcal{X}}^{(1)}$ and from $\mathcal{X}^{(2)}$ with the same label lie at the same region.

To evaluate our method numerically, we repeat the experiment reported in [14]. We train an SVM classifier on 10% of the local covariance matrices in $\tilde{\mathcal{X}}^{(1)}$ and test it on $\mathcal{X}^{(2)}$. We remark that pixels at the boundaries and pixels without enough valid neighbors for the covariance estimation are ignored. We consider only pixels with at least 500 valid neighbors, which applies to 95% of the labeled pixels. Figure 5 illustrates the classification results in the image plain, where pixels are colored according to their predicted class. We use the following Cohen’s kappa [8] to objectively evaluate the classification results:

$$\kappa = \frac{p_o - p_e}{1 - p_e}$$

where p_o is the classification accuracy and p_e is given by:

$$p_e = \frac{1}{N^2} \sum_k n_k^{(T)} n_k^{(P)}$$

where N is the number of observations to be classified, $n_k^{(T)}$ and $n_k^{(P)}$ is the true and predicted number of observation in class k , respectively. After applying Algorithm 5.1, the obtained Cohen’s kappa of the SVM classifier is $\kappa = 0.923$, while without DA it is only $\kappa = 0.550$.

Table 1: Comparison of the classification results after applying different DA algorithms. The column “Unsupervised” indicates that the algorithm does not require labels. The column “Unpaired” indicates that the algorithm is not restricted to images which are defined on a common grid. The column “Generic” indicates that the algorithm could be used for different datasets and is not specifically-tailored for HSI.

Algorithm	Unsupervised	Unpaired	Generic	κ (SVM)
NFNalign		✓		0.975
re-normalization	✓		✓	0.942
STCA		✓		0.901
KEMA		✓	✓	0.932
GFK	✓	✓	✓	0.920
Proposed	✓	✓	✓	0.923

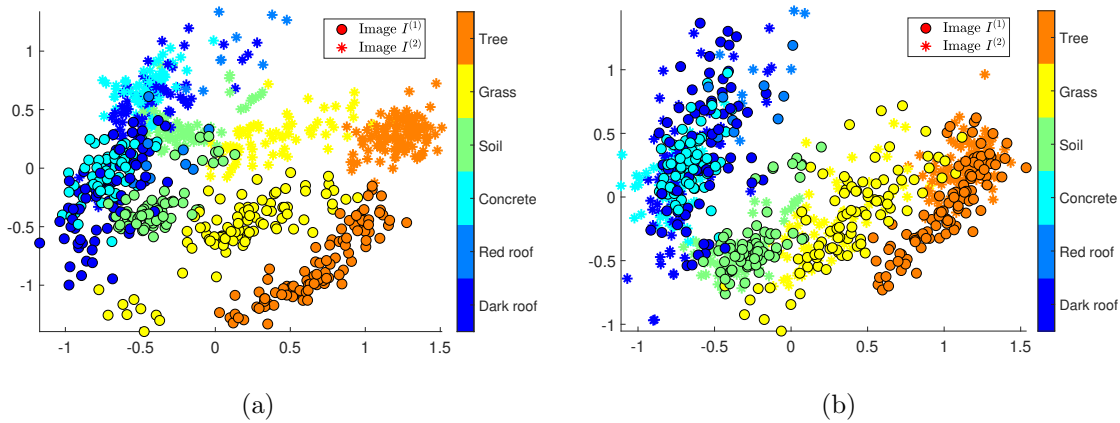


Figure 4: First 2 PC of 400 covariance matrices. Matrices computed in image $\mathbf{I}^{(1)}$ marked by circles, and matrices computed in image $\mathbf{I}^{(2)}$ marked by asterisks: (a) before DA, (b) after DA using Algorithm 5.1. Points are colored according to the land-cover classes.

Table 1 compares our results to other DA algorithms reported in [14]. We note that according to the reported setting in [14], the STCA, KEMA, GFK and NFNalign algorithms used the reflectance mode for image $\mathbf{I}^{(1)}$ and the radiance mode for $\mathbf{I}^{(2)}$, while the re-normalization and our algorithm used the reflectance mode for both images.

6.2. Motion recognition. In this experiment, we use the proposed method to apply domain adaption to the motion capture database HDM05 which is described in [24]. The HDM05 dataset contains more than 70 motion classes in 10 to 50 realizations executed by various actors. Some motions for example are: a cartwheel (left hand start), a clap (1 repetition), and a clap above head (1 repetition). The dataset contains recordings from five different actors that we denote for simplicity by Actor #1 to Actor #5. The data are acquired from 31 markers



Figure 5: Classification results. Labeled pixels are colored according to the predicted land-cover classes: (a) before DA, (b) after DA using Algorithm 5.1 and (c) ground truth.

that are attached to the actor’s body throughout the motion, see Figure 6(a). Specifically, each marker provides a 3D position at each time frame, see Figure 6(b). A single motion is about 3 second long recorded at 120Hz sampling rate. Overall, we write the i th motion of the k th actor as

$$\mathbf{m}_i^{(k)} = \mathbb{R}^{31 \times 3 \times T_i^{(k)}}$$

where the first dimension represents a specific marker, the second dimension represents the x, y, z coordinates, and $T_i^{(k)} \approx 360$ is the number of frames in the motion. From each motion $\mathbf{m}_i^{(k)}$, we compute the $\mathbf{X}_i^{(k)} \in \mathbb{R}^{93 \times 93}$ covariance matrix (by flattening the first two dimensions of $\mathbf{m}_i^{(k)}$ into a column stack vector). Empirically, we found that only four eigenvalues are consistently greater than zero for most $\mathbf{X}_i^{(k)}$. Thus, we set the fixed rank to $r = 4$, and as a consequence, we view the covariance matrices as points on $\mathcal{S}_{93,4}^+$.

To demonstrate the need for domain adaption between different actors, we take Actors #1 and #3 and consider all motions with more than 20 repetitions (combined). This provides us with the two sets $\{\mathbf{X}_i^{(1)}\}_{i=1}^{48}$ and $\{\mathbf{X}_i^{(3)}\}_{i=1}^{42}$. Figure 7(a) presents the 2D representation obtained by projecting the union $\{\mathbf{X}_i^{(1)}\}_{i=1}^{48} \cup \{\mathbf{X}_i^{(3)}\}_{i=1}^{42}$ to the tangent plane $\mathcal{T}_{\bar{\mathbf{C}}} \mathcal{S}_{d,r}^+$ where $\bar{\mathbf{C}}$ is the mean of the union using (4.1). Next, we apply tSNE [21] to the obtained vectors and using the induced metric by the inner product (2.16) with $k = 1$. Motions corresponding to Actor #1 are marked by circles (with black edges) and motions corresponding to Actor #3 are marked by asterisks. Different colors correspond to different motion types. We observe that the same motions by different actors do not reside in the same vicinity. To circumvent this undesired discrepancy we apply Algorithm 5.1 to $\{\mathbf{X}_i^{(1)}\}_{i=1}^{48}$ and $\{\mathbf{X}_i^{(3)}\}_{i=1}^{42}$ and obtain the new SPSP representation $\{\widetilde{\mathbf{X}}_i^{(1)}\}_{i=1}^{48}$. Figure 7(b) presents the 2D representation obtained

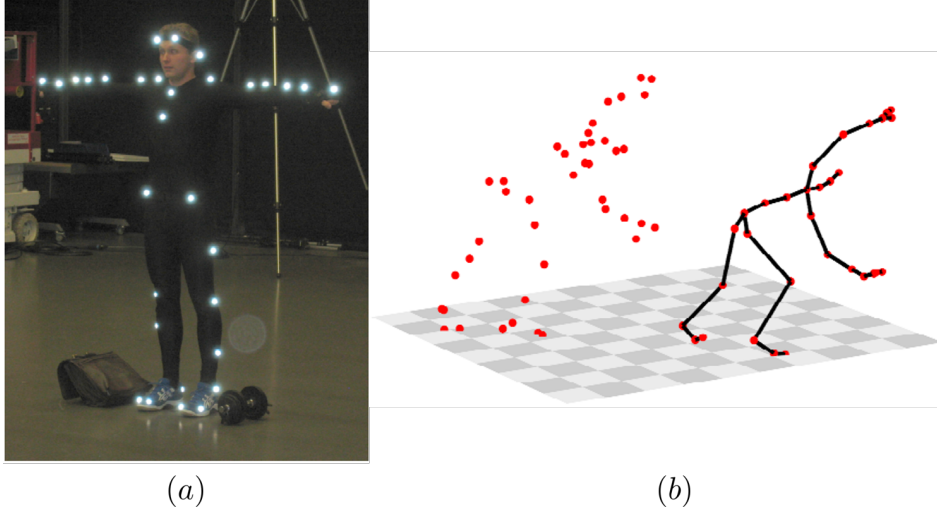


Figure 6: (a) The 31 markers attached to the actor’s body. (b) A frame from a cartwheel motion. Both images were taken from [24].

by applying tSNE to the union $\left\{ \widetilde{\mathbf{X}}_i^{(1)} \right\}_{i=1}^{48} \cup \left\{ \mathbf{X}_i^{(3)} \right\}_{i=1}^{42}$. We now observe that the same type of motions recorded from different actors reside in the same vicinity, thereby implying that we have achieved a meaningful DA between the two actors. Figure 8 is similar to Figure 7 but with Actors #2 and #3 (instead of #1 and #3). To provide quantitative results, we train linear SVM classifiers using the SPSP matrices of each actor and test the classification accuracy on all other actors. Specifically, given the two sets of SPSP matrices $\left\{ \mathbf{X}_i^{(k_1)} \right\}_i$ and $\left\{ \mathbf{X}_i^{(k_2)} \right\}_i$, the classifiers were trained in the tangent space $\mathcal{T}_{\overline{\mathbf{X}}} \mathcal{S}_{93,4}$ where $\overline{\mathbf{X}}$ is the mean of the union $\overline{\mathbf{X}} = M \left(\left\{ \mathbf{X}_i^{(k_1)} \right\} \cup \left\{ \mathbf{X}_i^{(k_2)} \right\} \right)$. We repeat this experiment twice, once before applying Algorithm 5.1 that is, we use $\left\{ \mathbf{X}_i^{(k_1)} \right\}_i$ and $\left\{ \mathbf{X}_i^{(k_2)} \right\}_i$, and once after applying Algorithm 5.1, that is, we use $\left\{ \widetilde{\mathbf{X}}_i^{(k_1)} \right\}_i$ and $\left\{ \mathbf{X}_i^{(k_2)} \right\}_i$. We note that we omit Actor #4 since the number of common motions between this actor and all other actors is too small. Table 2(a) presents the classification accuracy obtained before applying Algorithm 5.1. Table 2(b) presents the classification accuracy obtained after applying Algorithm 5.1. We observe that in all cases (except one) applying Algorithm 5.1 indeed improve the classification accuracy significantly.

7. Conclusions. Data analysis techniques using Riemannian geometry have proven to be useful in a broad range of fields. In this work, we extend existing results on the Riemannian geometry of SPSP matrices and establish a convenient framework for developing data analysis methods that rely on SPSP matrices as the data features. Notable examples for such features are (low rank) covariance matrices, various kernel matrices, and graph Laplacians. We demonstrate the usefulness of this framework and propose an algorithm for DA using PT on

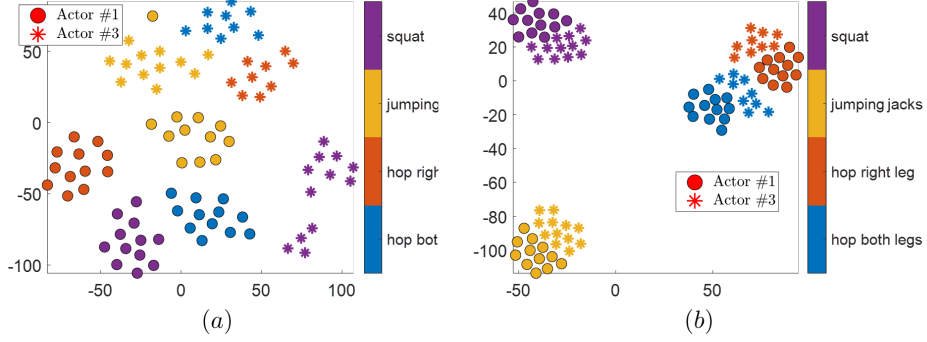


Figure 7: (a) 2D tSNE representation of the SPSP matrices $\{\mathbf{X}_i^{(1)}\}_{i=1}^{48} \cup \{\mathbf{X}_i^{(3)}\}_{i=1}^{42}$ (b) 2D tSNE representation of the SPSP matrices $\{\widetilde{\mathbf{X}}_i^{(1)}\}_{i=1}^{48} \cup \{\mathbf{X}_i^{(3)}\}_{i=1}^{42}$, where $\widetilde{\mathbf{X}}_i^{(1)}$ are the SPSP matrices obtained by Algorithm 5.1

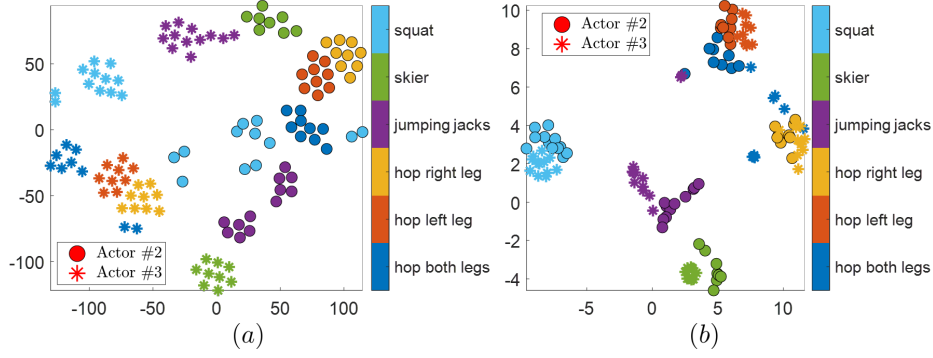


Figure 8: (a) 2D tSNE representation of the SPSP matrices $\{\mathbf{X}_i^{(2)}\}_{i=1}^{48} \cup \{\mathbf{X}_i^{(3)}\}_{i=1}^{42}$ (b) 2D tSNE representation of the SPSP matrices $\{\widetilde{\mathbf{X}}_i^{(2)}\}_{i=1}^{48} \cup \{\mathbf{X}_i^{(3)}\}_{i=1}^{42}$, where $\widetilde{\mathbf{X}}_i^{(2)}$ are the SPSP matrices obtained by Algorithm 5.1.

the manifold of SPSP matrices. We test the algorithm on two applications, hyper-spectral image fusion and motion identification, and observe good performance.

While the present work follows common practice and the experimental study focuses on covariance matrices, we intend in future work to examine other SPSP matrices. Perhaps the most significant future direction is the examination of graph Laplacians, which are inherently fixed-rank SPSP matrices and facilitate the representation of entire graphs as data features.

Acknowledgments. The data used in this project was obtained from HDM05 [24]. We thank Wolfgang Gross for making the data from [14] available.

Table 2: Motion recognition classification accuracy. (a) Classification without DA. Overall accuracy is 75.91% (b) Classification using [Algorithm 5.1](#). Overall accuracy is 96.73%.

Train \ Test	#1	#2	#3	#5
#1	92.36	45.83	96.00	
#2	97.62		95.83	95.83
#3	29.17	91.67		87.50
#5	98.75	95.83	83.33	

(a)

(b)

REFERENCES

- [1] P.-A. ABSIL, R. MAHONY, AND R. SEPULCHRE, Riemannian geometry of grassmann manifolds with a view on algorithmic computation, Acta Applicandae Mathematica, 80 (2004), pp. 199–220.
- [2] M. BACÁK, R. BERGMANN, G. STEIDL, AND A. WEINMANN, A second order nonsmooth variational model for restoring manifold-valued images, SIAM Journal on Scientific Computing, 38 (2016), pp. A567–A597.
- [3] A. BARACHANT, S. BONNET, M. CONGEDO, AND C. JUTTEN, Classification of covariance matrices using a riemannian-based kernel for bci applications, Neurocomputing, 112 (2013), pp. 172–178.
- [4] R. BERGMANN, J. H. FITSCHEN, J. PERSCH, AND G. STEIDL, Priors with coupled first and second order differences for manifold-valued image processing, Journal of mathematical imaging and vision, 60 (2018), pp. 1459–1481.
- [5] R. BHATIA, Positive definite matrices, vol. 24, Princeton university press, 2009.
- [6] S. BONNABEL, A. COLLARD, AND R. SEPULCHRE, Rank-preserving geometric means of positive semi-definite matrices, Linear Algebra and its Applications, 438 (2013), pp. 3202–3216.
- [7] S. BONNABEL AND R. SEPULCHRE, Riemannian metric and geometric mean for positive semidefinite matrices of fixed rank, SIAM Journal on Matrix Analysis and Applications, 31 (2010), pp. 1055–1070.
- [8] J. COHEN, A coefficient of agreement for nominal scales, Educational and psychological measurement, 20 (1960), pp. 37–46.
- [9] N. COURTY, R. FLAMARY, AND D. TUIA, Domain adaptation with regularized optimal transport, in Joint European Conference on Machine Learning and Knowledge Discovery in Databases, Springer, 2014, pp. 274–289.
- [10] N. COURTY, R. FLAMARY, D. TUIA, AND A. RAKOTOMAMONJY, Optimal transport for domain adaptation, IEEE transactions on pattern analysis and machine intelligence, 39 (2016), pp. 1853–1865.
- [11] C. DENG, X. LIU, C. LI, AND D. TAO, Active multi-kernel domain adaptation for hyperspectral image classification, Pattern Recognition, 77 (2018), pp. 306–315.
- [12] A. EDELMAN, T. A. ARIAS, AND S. T. SMITH, The geometry of algorithms with orthogonality constraints, SIAM journal on Matrix Analysis and Applications, 20 (1998), pp. 303–353.
- [13] L. FANG, N. HE, S. LI, A. J. PLAZA, AND J. PLAZA, A new spatial-spectral feature extraction method for hyperspectral images using local covariance matrix representation, IEEE Transactions on Geoscience and Remote Sensing, 56 (2018), pp. 3534–3546.
- [14] W. GROSS, D. TUIA, U. SOERGEL, AND W. MIDDELMANN, Nonlinear feature normalization for hyperspectral domain adaptation and mitigation of nonlinear effects, IEEE Transactions on Geoscience and Remote Sensing, 57 (2019), pp. 5975–5990.
- [15] A. HALIMI, P. HONEINE, M. KHAROUF, C. RICHARD, AND J. TOURNERET, Estimating the intrinsic

- dimension of hyperspectral images using a noise-whitened eigengap approach, *IEEE Transactions on Geoscience and Remote Sensing*, 54 (2016), pp. 3811–3821.
- [16] Z. HUANG, R. WANG, S. SHAN, X. LI, AND X. CHEN, Log-euclidean metric learning on symmetric positive definite manifold with application to image set classification, in *International conference on machine learning*, 2015, pp. 720–729.
 - [17] M.-D. IORDACHE, J. M. BIOUCAS-DIAS, AND A. PLAZA, Sparse unmixing of hyperspectral data, *IEEE Transactions on Geoscience and Remote Sensing*, 49 (2011), pp. 2014–2039.
 - [18] S. JAYASUMANA, R. HARTLEY, M. SALZMANN, H. LI, AND M. HARANDI, Kernel methods on riemannian manifolds with gaussian rbf kernels, *IEEE transactions on pattern analysis and machine intelligence*, 37 (2015), pp. 2464–2477.
 - [19] X. KANG, X. ZHANG, S. LI, K. LI, J. LI, AND J. A. BENEDIKTSSON, Hyperspectral anomaly detection with attribute and edge-preserving filters, *IEEE Transactions on Geoscience and Remote Sensing*, 55 (2017), pp. 5600–5611.
 - [20] A. KAPUR, K. MARWAH, AND G. ALTEROVITZ, Gene expression prediction using low-rank matrix completion, *BMC bioinformatics*, 17 (2016), p. 243.
 - [21] L. V. D. MAATEN AND G. HINTON, Visualizing data using t-sne, *Journal of machine learning research*, 9 (2008), pp. 2579–2605.
 - [22] G. MAMAN, O. YAIR, D. EYTAN, AND R. TALMON, Domain adaptation using riemannian geometry of spd matrices, in *ICASSP 2019-2019 IEEE International Conference on Acoustics, Speech and Signal Processing (ICASSP)*, IEEE, 2019, pp. 4464–4468.
 - [23] M. MOAKHER, A differential geometric approach to the geometric mean of symmetric positive-definite matrices, *SIAM Journal on Matrix Analysis and Applications*, 26 (2005), pp. 735–747.
 - [24] M. MÜLLER, T. RÖDER, M. CLAUSEN, B. EBERHARDT, B. KRÜGER, AND A. WEBER, Documentation mocap database hdm05, Tech. Report CG-2007-2, Universität Bonn, June 2007.
 - [25] Y. NIU AND B. WANG, Hyperspectral anomaly detection based on low-rank representation and learned dictionary, *Remote Sensing*, 8 (2016), p. 289.
 - [26] X. PENNEC, P. FILLARD, AND N. AYACHE, A riemannian framework for tensor computing, *International Journal of computer vision*, 66 (2006), pp. 41–66.
 - [27] P. RODRIGUES, F. BOUCHARD, M. CONGEDO, AND C. JUTTEN, Dimensionality reduction for bci classification using riemannian geometry, 2017.
 - [28] P. L. C. RODRIGUES, C. JUTTEN, AND M. CONGEDO, Riemannian procrustes analysis: transfer learning for brain-computer interfaces, *IEEE Transactions on Biomedical Engineering*, 66 (2018), pp. 2390–2401.
 - [29] A. SHRIVASTAVA, S. SHEKHAR, AND V. M. PATEL, Unsupervised domain adaptation using parallel transport on grassmann manifold, in *IEEE winter conference on applications of computer vision*, IEEE, 2014, pp. 277–284.
 - [30] R. WANG, H. GUO, L. S. DAVIS, AND Q. DAI, Covariance discriminative learning: A natural and efficient approach to image set classification, in *2012 IEEE Conference on Computer Vision and Pattern Recognition*, IEEE, 2012, pp. 2496–2503.
 - [31] C. WU, L. ZHANG, AND B. DU, Kernel slow feature analysis for scene change detection, *IEEE Transactions on Geoscience and Remote Sensing*, 55 (2017), pp. 2367–2384.
 - [32] O. YAIR, M. BEN-CHEN, AND R. TALMON, Parallel transport on the cone manifold of spd matrices for domain adaptation, *IEEE Transactions on Signal Processing*, 67 (2019), pp. 1797–1811.
 - [33] O. YAIR, F. DIETRICH, R. TALMON, AND I. G. KEVREKIDIS, Optimal transport on the manifold of spd matrices for domain adaptation, *arXiv preprint arXiv:1906.00616*, (2019).
 - [34] H. ZHANG, W. HE, L. ZHANG, H. SHEN, AND Q. YUAN, Hyperspectral image restoration using low-rank matrix recovery, *IEEE Transactions on Geoscience and Remote Sensing*, 52 (2013), pp. 4729–4743.

8. Supplementary materials.

Proposition 8.1. Let $\mathcal{X} = \{\mathbf{P}_i\}_i$ be a set of points on \mathcal{P}_d with the Riemannian mean $\overline{\mathbf{P}}$. Consider the map $t : \mathcal{P}_d \rightarrow \mathcal{P}_d$ defined by

$$\mathbf{R}_i = t(\mathbf{P}_i) = \mathbf{T} \mathbf{P}_i \mathbf{T}^T$$

where $\mathbf{T} \in \text{GL}_d$. Let $\overline{\mathbf{R}}$ be the Riemannian mean of the resulting set $\{\mathbf{R}_i\}_i$. The following holds

$$\Gamma_{\overline{\mathbf{P}} \rightarrow \overline{\mathbf{R}}}^+(\mathbf{P}_i) = \mathbf{R}_i, \quad \forall i$$

if and only if \mathbf{T} is of the form $\mathbf{T} = \overline{\mathbf{P}}^{\frac{1}{2}} \mathbf{B} \overline{\mathbf{P}}^{-\frac{1}{2}}$ where either $\mathbf{B} \succ 0$ or $\mathbf{B} \prec 0$.

Proof. Using the congruence invariance property of the geometric mean (see [5]), we have:

$$\overline{\mathbf{R}} = \mathbf{T} \overline{\mathbf{P}} \mathbf{T}^T$$

Note that

$$\begin{aligned} \mathbf{E} &= \left(\overline{\mathbf{R}} \overline{\mathbf{P}}^{-1} \right)^{\frac{1}{2}} \\ &= \left(\mathbf{T} \overline{\mathbf{P}} \mathbf{T}^T \overline{\mathbf{P}}^{-1} \right)^{\frac{1}{2}} \\ &= \left(\overline{\mathbf{P}}^{\frac{1}{2}} \overline{\mathbf{P}}^{-\frac{1}{2}} \mathbf{T} \overline{\mathbf{P}} \mathbf{T}^T \overline{\mathbf{P}}^{-\frac{1}{2}} \overline{\mathbf{P}}^{-\frac{1}{2}} \right)^{\frac{1}{2}} \\ &= \overline{\mathbf{P}}^{\frac{1}{2}} \left(\overline{\mathbf{P}}^{-\frac{1}{2}} \mathbf{T} \overline{\mathbf{P}} \mathbf{T}^T \overline{\mathbf{P}}^{-\frac{1}{2}} \right)^{\frac{1}{2}} \overline{\mathbf{P}}^{-\frac{1}{2}} \end{aligned}$$

First direction. Assume $\mathbf{T} = \overline{\mathbf{P}}^{\frac{1}{2}} \mathbf{B} \overline{\mathbf{P}}^{-\frac{1}{2}}$, then:

$$\begin{aligned} \mathbf{E} &= \overline{\mathbf{P}}^{\frac{1}{2}} \left(\overline{\mathbf{P}}^{-\frac{1}{2}} \mathbf{T} \overline{\mathbf{P}} \mathbf{T}^T \overline{\mathbf{P}}^{-\frac{1}{2}} \right)^{\frac{1}{2}} \overline{\mathbf{P}}^{-\frac{1}{2}} \\ &= \overline{\mathbf{P}}^{\frac{1}{2}} \left(\overline{\mathbf{P}}^{-\frac{1}{2}} \overline{\mathbf{P}}^{\frac{1}{2}} \mathbf{B} \overline{\mathbf{P}}^{-\frac{1}{2}} \overline{\mathbf{P}} \overline{\mathbf{P}}^{-\frac{1}{2}} \mathbf{B}^T \overline{\mathbf{P}}^{\frac{1}{2}} \overline{\mathbf{P}}^{-\frac{1}{2}} \right)^{\frac{1}{2}} \overline{\mathbf{P}}^{-\frac{1}{2}} \\ &= \overline{\mathbf{P}}^{\frac{1}{2}} (\mathbf{B} \mathbf{B}^T)^{\frac{1}{2}} \overline{\mathbf{P}}^{-\frac{1}{2}} \\ &= \pm \mathbf{T} \end{aligned}$$

There will be a $+$ sign if $\mathbf{B} \succ 0$ and a $-$ sign if $\mathbf{B} \prec 0$. Hence:

$$\Gamma_{\overline{\mathbf{P}} \rightarrow \overline{\mathbf{R}}}^+(\mathbf{P}_i) = \mathbf{E} \mathbf{P}_i \mathbf{E}^T = (\pm \mathbf{T}) \mathbf{P}_i (\pm \mathbf{T})^T = \mathbf{R}_i$$

Second direction. First, recall that

$$\mathbf{E} = \overline{\mathbf{P}}^{\frac{1}{2}} \left(\overline{\mathbf{P}}^{-\frac{1}{2}} \mathbf{T} \overline{\mathbf{P}} \mathbf{T}^T \overline{\mathbf{P}}^{-\frac{1}{2}} \right)^{\frac{1}{2}} \overline{\mathbf{P}}^{-\frac{1}{2}}$$

and let $\mathbf{B} := \left(\overline{\mathbf{P}}^{-\frac{1}{2}} \mathbf{T} \overline{\mathbf{P}} \mathbf{T}^T \overline{\mathbf{P}}^{-\frac{1}{2}} \right)^{\frac{1}{2}} \succ 0$ thus:

$$\mathbf{E} = \overline{\mathbf{P}}^{\frac{1}{2}} \mathbf{B} \overline{\mathbf{P}}^{-\frac{1}{2}}.$$

Hence, it is enough to show that

$$\mathbf{T} = \pm \mathbf{E} = \overline{\mathbf{P}}^{\frac{1}{2}} (\pm \mathbf{B}) \overline{\mathbf{P}}^{-\frac{1}{2}}.$$

Assume the mapping is exact, that is:

$$\mathbf{E} \mathbf{P}_i \mathbf{E}^T = \mathbf{T} \mathbf{P}_i \mathbf{T}^T, \quad \forall \mathbf{P}_i \in \mathcal{X}$$

then, without loss of generality, we consider $\mathbf{P}_i = \mathbf{I} \in \mathcal{X}$ for some i , and thus:

$$\mathbf{E} \mathbf{E}^T = \mathbf{T} \mathbf{T}^T$$

leading to

$$\mathbf{I} = \mathbf{E}^{-1} \mathbf{T} \mathbf{T}^T \mathbf{E}^{-T} = (\mathbf{E}^{-1} \mathbf{T}) (\mathbf{E}^{-1} \mathbf{T})^T$$

which implies that $\mathbf{E}^{-1} \mathbf{T} = \mathbf{U}$ is unitary. Now, from

$$\mathbf{E} \mathbf{P}_i \mathbf{E}^T = \mathbf{T} \mathbf{P}_i \mathbf{T}^T, \quad \forall \mathbf{P}_i \in \mathcal{X}$$

we have

$$\mathbf{P}_i = (\mathbf{E}^{-1} \mathbf{T}) \mathbf{P}_i (\mathbf{E}^{-1} \mathbf{T})^T = \mathbf{U} \mathbf{P}_i \mathbf{U}^T, \quad \forall \mathbf{P}_i \in \mathcal{X}$$

Again, without loss of generality, assume there exists $\mathbf{P}_j \in \mathcal{X}$ with unique eigenvalues, and thus, also with unique eigenvectors (up to a sign). Let \mathbf{v} and λ be an eigenvector and its corresponding eigenvalue, such that:

$$\mathbf{P}_j \mathbf{v} = \lambda \mathbf{v}$$

Since $\mathbf{P}_i = \mathbf{U} \mathbf{P}_i \mathbf{U}^T$ for all $\mathbf{P}_i \in \mathcal{X}$ we have

$$\implies \mathbf{U} \mathbf{P}_j \mathbf{U}^T \mathbf{v} = \lambda \mathbf{v}$$

and thus:

$$\mathbf{P}_j \mathbf{U}^T \mathbf{v} = \lambda \mathbf{U}^T \mathbf{v}$$

Since, the eigenvectors are unique, we have:

$$\mathbf{v} = \pm \mathbf{U}^T \mathbf{v}$$

Since this is true for the all the eigenvectors of \mathbf{P}_j we have:

$$\mathbf{U} = \pm \mathbf{I}$$

So that

$$\mathbf{E}^{-1} \mathbf{T} = \pm \mathbf{I}$$

which can be recast as

$$\mathbf{T} = \pm \mathbf{E}$$

■

Proposition 8.2. Let $\bar{Q} \in [\bar{Q}]$ and $\bar{V} \in [\bar{V}]$ be two points in \mathcal{O}_d , such that $\bar{V} = \Pi_{\bar{Q}}(\bar{V})$. Define $\Gamma_{\bar{Q} \rightarrow \bar{V}}^+ : \mathcal{G}_{d,r} \rightarrow \mathcal{G}_{d,r}$ by

$$(8.1) \quad \Gamma_{\bar{Q} \rightarrow \bar{V}}^+(Q_i) = \text{Exp}_{\bar{V}} \left(\Gamma_{\bar{Q} \rightarrow \bar{V}} \left(\text{Log}_{\bar{Q}}(Q_i) \right) \right)$$

Then

$$(8.2) \quad \Gamma_{\bar{Q} \rightarrow \bar{V}}^+(Q_i) \sim \Gamma_{\bar{Q} \rightarrow \bar{V}}(Q_i) = \bar{V} \bar{Q}^T Q_i$$

where \sim is the equivalent class, and if Q_i is chosen such that $Q_i = \Pi_{\bar{Q}}(Q_i)$, then the equivalence become equality:

$$(8.3) \quad \Gamma_{\bar{Q} \rightarrow \bar{V}}^+(Q_i) = \Gamma_{\bar{Q} \rightarrow \bar{V}}(Q_i) = \bar{V} \bar{Q}^T Q_i$$

Proof. Let

$$\bar{Q} B^{\text{skew}} = \text{Log}_{\bar{Q}}(Q_i) \in \mathcal{T}_{\bar{Q}} \mathcal{G}_{d,r}$$

Thus

$$\begin{aligned} \Gamma_{\bar{Q} \rightarrow \bar{V}}^+(Q_i) &= \text{Exp}_{\bar{V}} \left(\Gamma_{\bar{Q} \rightarrow \bar{V}} \left(\text{Log}_{\bar{Q}}(Q_i) \right) \right) \\ &= \text{Exp}_{\bar{V}} \left(\Gamma_{\bar{Q} \rightarrow \bar{V}} \left(\bar{Q} B^{\text{skew}} \right) \right) \\ &= \text{Exp}_{\bar{V}} \left(\bar{V} B^{\text{skew}} \right) \\ &= \bar{V} \exp \left(B^{\text{skew}} \right) \\ &= \bar{V} \bar{Q}^T \underbrace{\bar{Q} \exp \left(B^{\text{skew}} \right)}_{\sim Q_i} \\ &\sim \bar{V} \bar{Q}^T Q_i \end{aligned}$$

■